scientific reports

Check for updates

OPEN

Synthesis, anticancer evaluation, and electrochemical investigation of new chiral pyrazolo[4,3-*e*]tetrazolo[1,5-*b*][1,2,4]triazine sulfonamides

Mateusz Kciuk[1]✉, Gabriela Machura[2], Somdutt Mujwar[3], Beata Marciniak[1], Kamila Koszelska[2], Sylwia Smarzewska[2], Mariusz Mojzych[4] & Renata Kontek[1]

Pyrazolo[4,3-*e*]tetrazolo[1,5-*b*][1,2,4]triazine sulfonamides (MM-compounds) represent a novel class of heterocyclic compounds with promising anticancer potential. In this study, we report the synthesis and biological evaluation of two enantiomeric derivatives: the R-enantiomer (MM124) and the S-enantiomer (MM125). Both compounds exhibited potent and selective cytotoxicity against a panel of cancer cell lines derived from various tissue types, with a median IC_{50} value of 0.35 µM. Mechanistic investigations in colorectal (HT-29) and prostate (PC-3) cancer cell lines demonstrated that the compounds induce apoptosis, oxidative stress, and DNA damage. Electrochemical assays and computational studies further suggested that MM124 and MM125 interact with DNA. Additionally, in silico pharmacokinetic and toxicological profiling indicated favorable drug-like properties. These findings support the potential of MM124 and MM125 as candidates for the development of new anticancer agents, warranting further structural optimization and preclinical evaluation.

Keywords Cancer, Drug, Pyrazole, Tetrazole, Triazine

Abbreviations

5-FU	5-fluorouracil
ADMET	Absorption, distribution, metabolism, excretion, and toxicity
AO/EB	Acridine orange/ethidium bromide
ATCC	American type culture collection
ATR-IR	Attenuated total reflectance infrared spectroscopy
BBB	Blood–brain barrier
BDDE	Boron-doped diamond electrode
BTK	Bruton's tyrosine kinase
CDKs	Cyclin-dependent kinases
CHK1	Serine-protein kinase Chk1
CV	Cyclic voltammetry
CYP	Cytochrome P450
DAPI	4′,6-diamidino-2-phenylindole
DCF	2',7'-dichlorofluorescein
DCFH-DA	2,7-dichlorodihydrofluorescein diacetate
DMF	Dimethylformamide
DMSO	Dimethyl sulfoxide
DSBs	Double-strand breaks
dsDNA	Double-stranded DNA
ESI/MS	Electrospray ionization mass spectrometry

[1]Department of Molecular Biotechnology and Genetics, University of Lodz, Banacha 12/16, 90-237 Lodz, Poland. [2]Department of Inorganic and Analytical Chemistry, University of Lodz, 12 Tamka Str, 91-403 Lodz, Poland. [3]Chitkara College of Pharmacy, Chitkara University, Rajpura 140401, Punjab, India. [4]The Mazovian Academy in Płock, Collegium Medicum, Plac Dąbrowskiego 2, 09-402 Plock, Poland. ✉email: mateusz.kciuk@biol.uni.lodz.pl

FBS	Fetal bovine serum
FDA	Food and drug administration
FTIR	Fourier transform infrared
GI	Gastrointestinal absorption
GPF	Grid Parameter file
HE	Hoechst 33,342
hERG	Human ether-a-go-go-related gene
HRMS	High-resolution mass spectrometry
LMP	Low melting point agarose
LQTS	Long QT syndrome
MD	Molecular dynamics
MMP	Mitochondrial membrane potential
MTT	3-(4,5-dimethylthiazol-2-yl)-2,3-diphenyltetrazolium bromide
NMP	Normal melting point agarose
NMR	Nuclear magnetic resonance
NPT	Constant pressure simulation
PBLs	Peripheral blood lymphocytes
PBS	Phosphate buffered saline
PDB	Protein data bank
PDGFRα	Platelet-derived growth factor receptor α
P-gp	P-glycoprotein
PI	Propidium ioide
Q-TOF LC/MS	Qadrupole time-of-flight liquid chromatography-mass spectrometry
RFU	Relative fluorescence intensity units
rGyr	Radius of gyration
RMSD	Root mean square deviation
RMSF	Root mean square fluctuation
ROS	Reactive oxygen species
SD	Standard deviation
SEM	Standard error of the mean
SI	Selectivity index
SSBs	Single-strand breaks
SWV	Square-wave voltammetry
TLC	Thin-layer chromatography
TMS	Tetramethylsilane
TPSA	Topological polar surface area

Triazine constitutes an important scaffold in drug discovery. Depending on the position of the nitrogen atom three isomers of triazine can be distinguished: 1,2,3-triazines, 1,2,4-triazines, and 1,3,5-triazines[1]. 6-azauracil (2H-1,2,4-triazine-3,5-dione) was one of the first analogs of 1,2,4-triazine, which exhibited anticancer activity and was investigated in clinical trials. However, its clinical application was limited due to adverse side effects[2,3].

Tirapazamine (3-aminobenzo[*e*][1,2,4]triazine 1,4-dioxide) was another 1,2,4-triazine analog with cytotoxic activity associated with its conversion into toxic radicals, which induced single or double-strand DNA breaks (SSBs and DSBs) and apoptosis of treated cells[4,5]. In 2009, Gucký et al. synthesized 3,7-diarylo-5-(3,4,5-trimetoksyphenylo)pirazolo[4,3-*e*][1,2,4]triazine derivatives that exhibited cytotoxic activity towards multiple hematological and lung cancer cell lines[6]. Based on these findings Mojzych et. al synthesized various derivatives of the pyrazolo[4,3-*e*][1,2,4]triazines and assessed their biological activity in multiple cancer cell lines[7]. Various pyrazolo-triazines exhibited inhibitory activity towards histone deacetylases[8], metalloproteinases[9], tubulin[10], urease, and tyrosinase[11,12]. Tricyclic pyrazolo[4,3-*e*] [1, 2, 3]triazines fused with a triazole or tetrazole ring have emerged as an important class of pyrazolo-triazine derivatives with profound anticancer activity [7]. Furthermore, the incorporation of the sulfonamide group into the pyrazolo-triazine scaffold enabled the extension of the spectrum of potential molecular targets of the pyrazolo-triazne compounds[13] including ABL kinase[14,15], carbonic anhydrases[16], cyclin-dependent kinases (CDKs)[7,17], casein kinase 2 (CK2)[18,19], and glycogen synthase kinase 3 (GSK3)[20].

The pyrazolo[4,3-*e*][1,2,4]triazine derivatives are, so far, one of the least known groups of heterocycles. Nevertheless, the above literature data indicate that this structure has significant biological activity. Attachment of a tetrazole or triazole ring to the bicyclic structure of the pyrazolo[4,3-*e*][1,2,4]triazine and the addition of sulfonamide moiety can significantly improve the biological activity of compounds[7]. At present, numerous pyrazolo[4,3-*e*]tetrazolo[1,5-b][1,2,4]triazine derivatives undergo various phases of in vitro and in vivo studies (for the structural details of the compounds see **Table 8** of the discussion section).

For example, the most pre-clinically advanced derivative **MM129** was demonstrated to effectively limit cell viability via Bruton's tyrosine kinase (BTK) inhibition resulting in apoptosis of colorectal cancer cells in vitro. The activity of the compound was also evaluated in the zebrafish embryo xenograft model, where **MM129** showed synergistic anti-tumor activity with the chemotherapeutic agent – 5-fluorouracil (5-FU)[21]. Additionally, **MM129** exhibited good pharmacokinetics parameters and safety profile in mice[22]. Bukowski et al. evaluated the cytotoxic activity of **MM129** together with two other pyrazolo[4,3-*e*]tetrazolo[1,5-*b*][1,2,4]triazine sulfonamides **MM130**, and **MM131** in four cancer cell lines (cervical cancer (HeLa), colorectal cancer (HCT-116), prostate cancer (PC-3), and pancreatic cancer (BxPC-3), where the cytotoxic 50% inhibitory concentration (IC_{50}) of compounds ranged from 0.17–1.15 μM[23]. More recently, we have reported micromolar cytotoxicity of **MM134**, **MM136**,

MM137, and **MM139** compounds in BxPC-3, HCT-116, and PC-3 cells. Furthermore, the cytotoxic effect was selective for cancer cells and not normal human cells in vitro[24].

In this paper, we present the general method for the synthesis of two novel enantiomeric sulfonamide derivatives: the R-enantiomer (**MM124**) and the S-enantiomer (**MM125**) (Fig. 1) of the pyrazolo[4,3-*e*] tetrazolo[1,5-*b*][1,2,4]triazine ring system compound series incorporated with leucinol moiety and investigate their anticancer activity including cytotoxicity (for multiple cancer and normal cell lines of different tissue origin) as well as genotoxic, pro-apoptotic and pro-oxidative properties in HT-29 (colorectal adenocarcinoma) and PC3 (prostate cancer) cancer cell lines. Additionally, an electrochemical investigation was carried out to evaluate the DNA binding activity of the compounds. Molecular docking and molecular dynamics computation methods were employed to confirm the interaction between the compounds and DNA molecules.

Materials and methods

Synthesis of MM124 and MM125

Melting points were determined on a Mel-Temp apparatus and were uncorrected. ^{1}H and ^{13}C nuclear magnetic resonance (NMR) spectra were recorded on a Varian spectrometer (400 MHz for ^{1}H and 100 MHz for ^{13}C). The chemical shift values were expressed in ppm (part per million) with tetramethylsilane (TMS) as an internal reference. The relative integrals of peak areas agreed with those expected for the assigned structures. The molecular weight of the final compounds was assessed by electrospray ionization mass spectrometry (ESI/MS) on Agilent Technologies 6538 UHD Accurate mass qadrupole time-of-flight liquid chromatography-mass spectrometry (Q-TOF LC/MS) (Warsaw, Poland). The attenuated total reflectance infrared spectroscopy (ATR-IR) spectra were recorded over the range of 4000–400 cm^{-1} on the Thermo Scientific Nicolet 6700 Fourier transform infrared (FTIR) spectrophotometer. Elemental compositions were within ± 0.4% of the calculated values. For preparation and spectroscopic data of compounds **1** see the literature[25].

The synthesis of the key tricyclic compounds with a sulfonamide moiety (**MM124** and **MM125**) was performed by the standard procedure described in our previous articles[7,24,26] (Fig. 2). Briefly, the known chlorosulfonyl derivative **1** was reacted with enantiomeric leucinols to give the two corresponding chiral derivatives **2ab**, which, when reacted with sodium azide in anhydrous ethanol under reflux, provided the final designed tricyclic sulfonamides **MM124** and **MM125**. The structure and purity of the newly synthesized compounds were characterized by ^{1}H and ^{13}C NMR and high-resolution mass spectrometry (HRMS) methods along with elemental and ATR-IR analysis (provided in the supplementary material – **SM1**).

Synthesis of sulfonamides (2ab)

Reaction (a): Derivative 1 (194 mg, 0.5 mmol) was dissolved in anhydrous acetonitrile (5 mL) and the appropriate amount of pure *S* or *R* enantiomer of leucinol (1.75 mmol) was added. The reaction was stirred overnight at room temperature, and then the reaction mixture was concentrated *in vacuo* to afford the crude sulfonamide, as a yellow solid. The residue was purified on silica gel using a mixture of CH_2Cl_2:EtOH (25:1) as eluent to give the titled compounds as a yellow solid.

Synthesis of N-(R)-(1-hydroxy-4-methyl-pent-2-yl)-4-(3-methyl-5-methylsulfonyl-1H-pyrazolo[4,3-e][1,2,4] triazyn-1-yl)benzenesulfonamide (2a)

Yield 98%. Melting point: 138–142 °C; IR cm^{-1}: 3503, 2933, 1596, 1505, 1456, 1410, 1313, 1147, 1094, 950, 826, 727, 612; ^{1}H NMR (DMSO) δ: 0.59 (d, 3H, J = 6.4 Hz), 0,75 (d, 3H, J = 6.8 Hz), 1.10–1.17 (m, 1H), 1.28–1.35

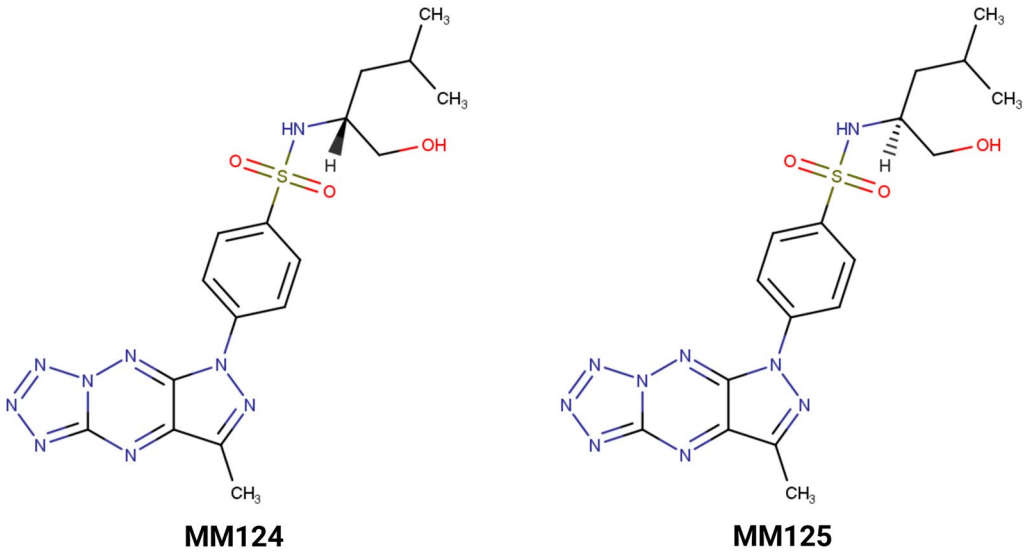

Fig. 1. Chemical structure of two investigated enantiomeric sulfonamides **MM124** (R-enantiomer) and **MM125** (S-enantiomer) incorporated with leucinol moiety.

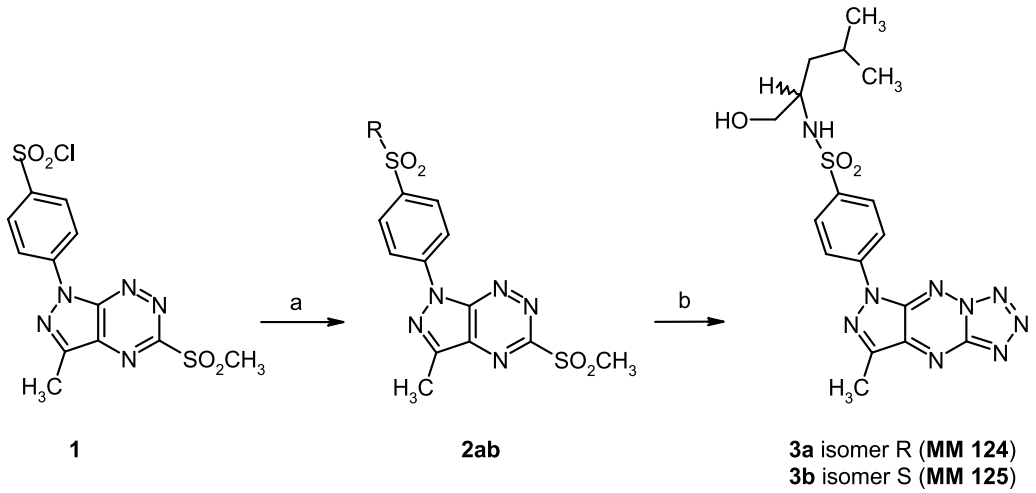

Fig. 2. Reagents and conditions: (**a**) appropriate leucinol, MeCN, rt, 3 h; (**b**) NaN3, EtOH, reflux. For the details see the main text below.

(m, 1H). 1.48–1.55 (m, 1H), 2.79 (s, 3H), 3.10–3.17 (m, 2H), 3.28 (t, 1H, J = 5.6 Hz), 3.62 (s, 3H), 4.66 (t, 1H, J = 5.2 Hz, exchanged with D_2O, OH), 7.65 (d, 1H, J = 7.2 Hz, exchanged with D_2O, NH), 8.10 (d, 2H, J = 8.8 Hz), 8.53 (d, 2H, J = 8.8 Hz); ^{13}C NMR (DMSO) δ: 11.12, 21.46, 23.35, 23.68, 40.53, 40.83, 53.43, 64.12, 120.00, 128.39, 138.24, 140.12, 140.26, 146.08, 148.30, 160.96; HRMS (ESI, m/z) Calcd for $C_{18}H_{24}N_6O_5S_2$ [M^+ + H] 469.13224. Found [M^+ + H] 469.13293. Anal. Calcd for $C_{18}H_{24}N_6O_5S_2$: C, 46.14; H, 5.16; N, 17.94. Found: C, 46.25; H, 5.32; N, 17.72.

Synthesis of N-(S)-(1-hydroxy-4-methyl-pent-2-yl)-4-(3-methyl-5-methylsulfonyl-1H-pyrazolo[4,3-e][1,2,4] triazyn-1-yl)benzenesulfonamide (2b)
Yield 82%. Melting point: 141–145 °C; IR cm^{-1}: 3493, 2933, 1596, 1506, 1313, 1150, 968, 727, 612; ^{1}H NMR (DMSO) δ: 0.59 (d, 3H, J = 6.4 Hz), 0,76 (d, 3H, J = 6.4 Hz), 1.10–1.19 (m, 1H), 1.28–1.35 (m, 1H). 1.45–1.55 (m, 1H), 2.79 (s, 3H), 3.10–3.17 (m, 2H), 3.27 (m, 1H), 3.62 (s, 3H), 4.66 (t, 1H, J = 5.6 Hz, exchanged with D_2O, OH), 7.65 (d, 1H, J = 7.2 Hz, exchanged with D_2O, NH), 8.10 (d, 2H, J = 8.8 Hz), 8.53 (d, 2H, J = 8.8 Hz); ^{13}C NMR (DMSO) δ: 11.83, 22.22, 23.99, 24.57, 41.13, 41.59, 54.13, 64.78, 121.27, 129.14, 138.90, 140.64, 141.03, 147.37, 148.89, 161.50; HRMS (ESI, m/z) Calcd for $C_{18}H_{24}N_6O_5S_2$ [M^+ + H] 469.13224. Found [M^+ + H] 469.13286. Anal. Calcd for $C_{18}H_{24}N_6O_5S_2$: C, 46.14; H, 5.16; N, 17.94. Found: C, 46.30; H, 5.28; N, 17.78.

Synthesis of tricyclic sulfonamides (3ab—MMs)
Reaction (b): A sulfonamide derivative with a methylsulfonyl group (0.33 mol) was dissolved in anhydrous ethanol (5 mL), and sodium azide (26 mg, 0.4 mol) was added. The reaction mixture was refluxed until the substrate disappeared (control thin-layer chromatography (TLC)). Then, the solvent was evaporated and the crude product was purified using column chromatography and CH_2Cl_2: MeOH (50:1) mixture as eluent to give the final compounds as a yellow solid.

N-(R)-(1-hydroxy-4-methyl-pent-2-yl)-4-[7-methyl-5H-pyrazolo[4,3-e]tetrazolo[4,5-b][1,2,4]triazin-5-yl)] benzenesulfonamide (3a: MM-124)
Yield 76%. Melting point: 157–160 °C; IR cm^{-1}: 3406, 3161, 2926, 1592, 1507, 1461, 1411, 1320, 1142, 1095, 969, 832, 643; ^{1}H NMR (methanol) δ: 0.66 (d, 3H, J = 6.4 Hz), 0,81 (d, 3H, J = 6.8 Hz), 1.18–1.26 (m, 1H), 1.32–1.38 (m, 1H), 1.48–1.55 (m, 1H), 2.85 (s, 3H), 3.24–3.30 (m, 1H), 3.30–3.35 (m, 1H), 3.42–3.45 (m, 1H), 4.57 (t, 1H, J = 5.6 Hz, OH), 8.08 (d, 2H, J = 8.8 Hz), 8.43 (d, 2H, J = 8.8 Hz); ^{13}C NMR (methanol) δ: 11.19, 22.05, 23.62, 25.34, 42.02, 54.88, 65.95, 120.13, 129.68, 140.88, 141.86, 143.30, 148.33, 148.88, 149.30; HRMS (ESI, m/z) Calcd for $C_{17}H_{21}N_9O_3S$ [M^+ + H] 432,48,235. Found [M^+ + H] 432,48,276. Anal. Calcd for $C_{17}H_{21}N_9O_3S$: C, 47.32; H, 4.91; N, 29.22. Found: C, 47.49; H, 5.08; N, 29.00.

N-(S)-(1-hydroxy-4-methyl-pent-2-yl)-4-[7-methyl-5H-pyrazolo[4,3-e]tetrazolo[4,5-b][1,2,4]triazin-5-yl)] benzene-sulfonamide (3b: MM-125)
Yield 88%. Melting point: 159–161 °C; IR cm^{-1}: 3411, 3158, 2923, 1592, 1506, 1460, 1411, 1319, 1151, 1095, 970, 853, 832, 725, 643; ^{1}H NMR (methanol) δ: 0.66 (d, 3H, J = 6.4 Hz), 0,81 (d, 3H, J = 6.4 Hz), 1.20–1.26 (m, 1H), 1.32–1.38 (m, 1H), 1.48–1.55 (m, 1H), 2.85 (s, 3H), 3.25–3.35 (m, 2H), 3.42–3.46 (m, 1H), 4.57 (bs, 1H, OH), 8.08 (d, 2H, J = 8.8 Hz), 8.43 (d, 2H, J = 8.8 Hz); ^{13}C NMR (methanol) δ: 11.18, 22.05, 23.62, 25.35, 42.03, 54.89, 65.96, 120.13, 129.70, 140.91, 141.86, 143.32, 148.33, 148.87, 149.31; HRMS (ESI, m/z) Calcd for $C_{17}H_{21}N_9O_3S$ [M^+ + H] 432,48,235. Found [M^+ + H] 432,48,282. Anal. Calcd for $C_{17}H_{21}N_9O_3S$: C, 47.32; H, 4.91; N, 29.22. Found: C, 47.55; H, 4.88; N, 29.05.

Biological studies

Chemicals

Trypsin–EDTA and all culture media (RPMI-1640, DMEM-F12, MEM) were purchased from Biowest (CytoGen, Poland). EMEM medium was purchased from the American Type Culture Collection (ATCC, Rockville, USA). 4′,6-diamidino-2-phenylindole (DAPI), acridine orange/ethidium bromide (AO/BE), propidium iodide (PI), Hoechst 33,342 (HE), bleomycin, phosphate-buffered saline (PBS), dimethylformamide (DMF), penicillin–streptomycin solution stabilized, fetal bovine serum (FBS), histopaque1077, dimethyl sulfoxide (DMSO), 3-(4,5-dimethylthiazol-2-yl)-2,3-diphenyltetrazolium bromide (MTT), normal melting point agarose (NMP), low melting point agarose (LMP), sodium dodecyl sulfate (SDS), Triton X-100 were supplied by Sigma Aldrich Chemical Co (USA). MitoTracker Red was purchased from Invitrogen (UK). 5-fluorouracil (5-FU) was obtained from MedChemExpress LLC (TriMen Chemicals, Lodz, Poland).

Cell culture

Cancer cell lines: BxPC-3 (pancreas adenocarcinoma, ATCC® CRL-1687™), DLD-1 (colorectal adenocarcinoma, ATCC CCL-221 ™), HCT-116 (colorectal carcinoma, ATCC® CCL-247™), HT-29 (colorectal adenocarcinoma, ATCC® HTB-38™) and PC3 (prostate cancer, ATCC® CRL-1435™) and normal cell lines: CCD 841 CoN (large intestine normal cells, CRL-1790 ™) and WI-38 (human lung fibroblasts, ATCC® CCL-75™) were obtained from American Type Culture Collection (ATCC). The MycoBlue™ Mycoplasma Detector kit (Vazyme Biotech Co., Ltd., Nanjing, China) was used at least every month for the control of mycoplasma contamination in the cell cultures. The human peripheral blood lymphocytes (PBLs) were isolated from leucocyte buffy-coat obtained from blood collection at the Blood Bank in Lodz, Poland. Blood came from healthy, non-smoking donors (adults, aged 25–40) who had no signs of infection during collection. The use of a human leucocyte buffy-coat was approved by the Bioethics Committee for Scientific Investigation, University of Lodz (agreement no. KBBN-UŁ/I/8/2019). PBLs were isolated from blood by centrifugation in a density gradient of Histopaque®1077 (300 g for 25 min). The obtained pellet was resuspended in RPMI-1640 medium to the density of about $1–3 \times 10^5$ cells per mL. Lymphocytes were grown in RPMI-1640 medium with 10% (v/v) FBS, 1% (v/v) penicillin–streptomycin, and phytohaemagglutinin (PHA). Adherent cells were cultured in dedicated cell media as shown in Table 1.

MTT assay

MTT cytotoxicity assay is a common method for determining the metabolic activity in living cells. The assessment is based on the enzymatic conversion of a tetrazolium salt that has a light color to its purple-blue formazan product that can be quantified using spectrophotometry. The obtained absorbance value is directly proportional to the metabolically active cells in the sample[27,28].

96-well plates were seeded at a density of approximately 8×10^3 (DLD-1, HCT-116, HT-29 cells), 1×10^4 (CCD 841 CoN, BxPC-3, PC3, and WI-38), and 8×10^4 (PBL_s) cells per 100 µL medium per well. After 24-h incubation in controlled conditions (37 °C; 5% CO_2), cells were exposed to tested **MM**-compounds in the range of 0.1–5 µM. These concentrations were obtained by diluting the compounds in DMSO (final concentration was < 0.5% *v/v*)[29] and in the culture medium. 5-FU was used in the concentration range of 2–500 µM.

The experimental design included non-treated controls and blanks (wells without cells).

After 72-h of incubation, 20 µl of MTT tetrazolium salt (5 mg/mL in PBS) was added to each well, and plates were incubated in a humidified atmosphere for 3 h (37 °C; 5% CO_2).

The solutions were removed and 100 µL of DMSO was added to dissolve formazan complexes in case of adherent cancer cells or by directly adding a 100 µL mixture of 20% SDS and 50% DMF to each well for 24 h PBL_s. A spectrophotometer (microplate reader Power Wave XS BioTek Instruments, Inc., USA) reading was performed at 570 nm.

A statistical program (*GraphPad Prism 7*) was used to analyze the obtained data. The dose–response analysis was performed to estimate the inhibitory concentration (IC_{50}) of tested compounds. The IC_{50} value is defined as a concentration of tested compound that leads to a reduction of cell pool viability by 50% compared to the negative control (accepted as 100%).

$$\%\ cell\ viability = \frac{(Absorbance\ value\ of\ treated\ cells - Absorbance\ value\ of\ blank)}{(Absorbance\ value\ of\ untreated\ cells - Absorbance\ value\ of\ blank)} \times 100\%$$

The selectivity index (SI) was calculated as a ratio of median IC_{50} values in normal cell lines and cancer cell lines.

Type of cells	Medium	Supplements
BxPC-3 DLD-1 HCT-116 HT-29	RPMI-1640	10% (v/v) FBS, 1% penicillin–streptomycin
PC-3	DMEM-F12	
CCD 841 CoN	EMEM	
WI-38	MEM	

Table 1. Composition of culture media used to cultivate adherent cells.

$$\mathrm{SI} = \frac{(Median\ IC50\ value\ calculated\ for\ normal\ cell\ lines)}{(Median\ IC50\ value\ calculated\ for\ cancer\ cell\ lines)}$$

MitoTracker Red – mitochondrial membrane potential changes ($\Delta\Psi m$)
MitoTracker Red is a derivative of dihydro-X-rosamine. Reduced MitoTracker dyes undergo oxidation in the viable cells, and form conjugates with thiol groups of proteins which make them fluorescent[30]. The intensity of fluorescence correlates with the fitness of the mitochondria and changes with alterations in mitochondrial membrane potential (MMP)[31].

Tumor (HT-29 and PC-3) cells were seeded at a density of 2×10^4 on 96-well black clear-bottom plates. Cells were incubated with 0.5, 1, and 2 μM concentrations of **MM124** and **MM125** for 24 h. After 24-h cells were incubated with MitoTracker Red (0.1 μM/200 μL PBS/well) for 40 min. After incubation time MitoTracker Red solution was discarded and PBS (200 μL/well) was added. Fluorescence was read at an absorbance/emission of 581/644 nm using the SpectraMax® i3x Multi-Mode Detection Platform.

Dual acridine orange/ethidium bromide (AO/EB) and propidium iodide/Hoechst 33,342 (PI/HE) double staining
Tumor HT-29 and PC-3 cells were seeded at a density of 1.5×10^5 on 12-well plates Following 24 h, cells were exposed to **MM124** and **MM125** in 0.5, 1, and 2 μM concentrations for 24 h. Following the incubation period, cells were incubated with fluorochromes (AO/EB: 100 μM; 1:1, v/v) or (PI/HE: 1 μg/mL; 1:1, v/v) for 5 min at 37 °C in the dark. Cells were examined in a fluorescence microscope (Olympus BX60 F5 Olympus Optical Co.Ltd.) at 360 nm. The results were obtained in duplicates and presented as mean percentage of necrotic and apoptotic cells ± standard deviation (SD) values. The differences between the experimental samples and control samples were estimated by the ANOVA test followed by the post-hoc Dunnetts test ($p < 0.05$, $N = 200$).

Study of reactive oxygen species (ROS) formation
Assessment of intracellular levels of reactive oxygen species (ROS) was carried out using a fluorescent probe 2,7-dichlorodihydrofluorescein diacetate (DCFH-DA). The DHCF-DA probe is hydrolyzed by intracellular esterases after penetrating the cell membrane. The resulting product is oxidized in the presence of oxidants such as H_2O_2, ·OH, ·NO_2, and others, to the highly fluorescent 2',7'-dichlorofluorescein (DCF). This allows fluorescence emission in a population of cells to be measured or identified microscopically[32,33].

HT-29 and PC-3 cells were seeded on 96-well black microplates at density 12×10^5/mL and cultured in standard conditions (37 °C; 5% CO_2) for about 48 h until they reached the exponential growth phase. After this time, the culture medium was removed and the cells were washed three times with PBS. A 20 μM DCFH-DA solution (in PBS) was then applied and the cells were incubated for 20 min. Subsequently, the fluorescent probe was removed and cells were washed with PBS again. Solutions of **MM124** and **MM125** were applied at concentrations equivalent to 0.5xIC_{50}, IC_{50}, and 2xIC_{50} values obtained in the MTT assay. Negative control cells were incubated with PBS, and the positive control included cells treated with H_2O_2 at a concentration of 500 μM. Fluorescence was measured on reader SpectraMax i3 Molecular Devices using an excitation wavelength of 485 nm and emission of 535 nm following 120 min.

Genotoxicity studies
The comet assay is a commonly used method for measuring DNA strand breaks at a single-cell level. The method stems from the simple principle that DNA fragmented following treatment with a genotoxic compound migrates more quickly than undamaged DNA in agarose gel during electrophoresis. In summary, single-cell suspensions mixed with LMP are layered on microscope slides covered in NMP, then lysed with detergent to rupture cell membranes and remove histone proteins, and finally electrophoresed to separate the fragmented DNA from intact DNA. In the presence of strand breaks, DNA moves in the direction of the anode, creating a picture that, when stained with a fluorescent dye and viewed using a fluorescence microscope, resembles the tail of a comet. Alkaline comet assay allows easy estimation of SSBs and apurinic/apyrimidinic sites[34–37].

The alkaline version of the comet assay was used in the current study according to Singh et al. (1988)[38], with modifications. Cells were seeded at a density of 150 000/2 mL (HT-29), 250 000/2 mL (PC3), and 600 000/2 mL of PBL_s onto 6-well plates. Following 24 h, cells were subjected to **MM124** and **MM125** in 0.5 μM, 1 μM, and 2 μM concentrations. Untreated control and positive control (cells treated with 20 μM bleomycin) were used in the experiment. Cells were exposed to compounds for another 24 h (37 °C; 5% CO_2). Afterward, they were transferred to Eppendorf tubes and centrifuged at 1400 rpm for 10 min at 4 °C. The precipitate was diluted in PBS. The next steps were performed as it was previously described by our group[23,24]. Following electrophoresis, slides were stained with DAPI (1 μg/ml) and coverslipped. DNA damage was evaluated with the use of fluorescence microscopy at 360 nm using *CellSens* (Olympus) software. A total number of approximately 100 cells per slide was chosen for further analysis.

CASP: Comet Assay Software Project Lab (http://casplab.com) software was used to establish the mean value of DNA (%) in comet tails. The data were presented with a standard error of the mean (± standard error of the mean; SEM) and analyzed with ANOVA followed by post-hoc Dunnett's test ($p < 0.05$, $N = 200$).

Electrochemical studies

Chemicals and reagents
Stock solutions of **MM124** and **MM125** were prepared by dissolving the required amount of the analytes in DMSO. Lower concentrations were achieved by properly diluting the stock sulfonamide derivatives solutions. The voltammetric analysis utilized PBS as a supporting electrolyte with a pH of 7.4. Both PBS and double-stranded salmon sperm DNA (dsDNA) were supplied from Sigma Aldrich Chemical Co (USA). A standard

stock solution of DNA was prepared by dissolving the requisite amount of DNA powder in PBS. Aqueous solutions were made using distilled and deionized water.

Apparatus and instrumentation

Electrochemical measurements were performed using a versatile potentiostat EmStat3 (PalmSens, the Netherlands), run by the PS Trace software (version no. 5.9). A traditional three-electrode system was used, with a boron-doped diamond electrode (Redoxme AB, Sweden, diameter: 2 mm) as a working electrode, a platinum wire (Mineral, Poland) used as an auxiliary electrode, and an Ag/AgCl electrode (Mineral, Poland) used as a reference electrode. During all experiments, a voltammetric cell of 10 mL was used. The pH of the supporting electrolytes was measured using a pH meter (Elmetron, Poland) equipped with a combination glass electrode.

Electrochemical measurements

In the present study square-wave (SWV) and cyclic voltammetry (CV) were applied for the general characterization of the chosen sulfonamide derivatives (**MM124**, **MM125**). Whereas, interaction studies were performed using SW voltammetry. Interaction studies were performed as follows: measurements of **MM124**, and **MM125** (at their fixed concentrations) were performed in the presence and absence of dsDNA in PBS at pH 7.4. 10 ml of a chosen supporting electrolyte was introduced in an electrochemical cell and then purged with argon for 5 min. After recording the voltammogram of the pure PBS, precise amounts of **MM124** or **MM125** and dsDNA were added using a micropipette. Following each addition, the solution underwent another 15-s deoxygenation, and a voltammogram was again recorded. The working electrode surface (boron-doped diamond electrode; BDDE) was polished with alumina slurry suspension on a polishing cloth before each voltammetric measurement. After that, the electrode surface was rinsed with distilled water. All experiments were performed in triplicate. The SWV conditions used during the experiments were as follows: amplitude of 25 mV, step potential of 5 mV, and frequency of 25 Hz. Cyclic voltammograms were obtained using a scan rate of 50–500 mV s^{-1}.

Computational analysis

Drug likeness and ADMET

The oral drug-likeness of compounds (here **MM124** and **MM125**) can be predicted using *SwissADME* (http://www.swissadme.ch/). Based on several assumptions (parameters) referred to as Lipinski's rule of five: (a) octanol/water partition coefficient (log P) of the molecule not be greater than five, (b) molecular weight less than 500 Da, (c) not more than five hydrogen bond donors, (d) and no more than 10 hydrogen bond acceptors a drug-likeness of the compound can be estimated. In contrast, bioavailability can be predicted based on several features of compounds, including flexibility (no more than 9 rotatable bonds), lipophilicity (XLOGP3 parameter between − 0.7 and + 5.0), size: molecular weight (between 150 and 500 g/mol), polarity (topological polar surface area (TPSA) between 20 and 130 Å2), solubility (LogS not higher than 6), and saturation (fraction of carbons in the sp3 hybridization (Csp3) not less than 0.25).

Moreover, key parameters including gastrointestinal absorption (GI), blood–brain barrier (BBB) permeability, cytochrome P450 3A4 (CYP3A4) and cytochrome P450 2D6 (CYP2D6) inhibition potential and toxicity can be predicted using pkCSM (http://biosig.unimelb.edu.au/pkcsm/)[39], SwissADME[40] and PreADMET online servers (https://preadmet.qsarhub.com/). Additionally, multiple toxicological features including hepatotoxicity, carcinogenicity, immunotoxicity, mutagenicity, and cytotoxicity can be predicted using Protox-II (http://tox.charite.de/protox_II).

Molecular docking

A crystallized structural model of the 6-BP DNA molecule complexed with ellipticine was revealed by X-ray crystallography technique at a resolution of 1.50 Å (PDB code: 1Z3F)[41].

The structure model comprises a dsDNA molecule with the intercalating agent. The DNA molecule was prepared for docking analysis by the addition of polar hydrogen, Gasteiger charge, and assigning autodock atom type, while the complex ligand was prepared by providing the flexibility followed by saving both in the default PDBQT format of Autodock software. Grid-box was prepared by covering the extended conformations of the reference ligand ellipticine as well as the interacting residues of the DNA and the grid parameters used in the current docking analysis are tabulated in Table 2.

The docking analysis was conducted using the Lamarckian Genetic Algorithm (LGA), employing a population size of 150, 2.5 million energy evaluations, and 27,000 generations across 30 independent runs for each ligand. The docking protocol and parameters were validated by re-docking the reference ligand to the target DNA. Validation criteria included the comparison of binding scores, structural alignment, and chemical interactions to confirm that the docking simulation accurately reproduced the binding mode observed in the reference bioactive complex. The validated docking parameters were further utilized for the docking of the **MM124** and **MM125** compounds with the intent to identify their DNA interacting properties that could explain the genotoxic potential of the compounds.

Target	PDBid	x-axis	y-axis	z-axis	Spacing (Å)	x center	y center	z center
DNA	1Z3F	40	40	44	0.397	-0.22	16.784	46.015

Table 2. The coordinates of the grid box used in the **MM124** and **MM125** in silico DNA interactions studies.

Molecular dynamics simulation

The obtained docking results were further validated for the stability of the macromolecular drug-receptor complex concerning time by performing molecular dynamics (MD) simulations. MD simulation was executed for each of the above-mentioned macromolecular complexes for 100 ns by using the Desmond module of Schrodinger's Maestro software[34–37]. Addition of explicit solvent molecules followed by their neutralization by adding the respective ions. The steepest-descent algorithm was used to relax the system and eliminate any steric clashes or poor contacts within atoms to minimize the system's energy. Using a short series having low temperature with constant pressure (NPT) simulations, the system was brought to equilibrium. Positional constraints were applied to the system in addition to a progressive increase in temperature which usually makes it more likely that the system will be in a stable, balanced state before the simulation. To get the appropriate outcomes, the simulation was performed for 100 ns while taking into account the system's energies, atom positions, and deviation values[42–44].

Results

Biological studies

MTT assay

MTT assay used to determine the cytotoxicity of compounds showed that both **MM124** and **MM125** possess cytotoxic activity towards tested cell lines (Table 3). **MM124** compound exhibited the highest cytotoxic activity towards HT-29 colorectal cancer cells ($IC_{50} = 0.22 \pm 0.02$ µM) and PC-3 cells ($IC_{50} = 0.3$ µM), while showing lower cytotoxicity in normal human colon tissue cells (CCD 841 CoN) ($IC_{50} = 1.12 \pm 0.04$ µM), human fibroblasts (WI-38 cells) ($IC_{50} = 0.98 \pm 0.13$ µM) and PBLs ($IC_{50} = 0.87 \pm 0.07$ µM). In contrast, **MM125** exerted the highest activity in HT-29 cells ($IC_{50} = 0.27 \pm 0.02$ µM) and pancreatic cancer (BxPC-3) cells ($IC_{50} = 0.21 \pm 0.02$ µM). Similarly, to the other investigated derivative, **MM125** showed preferential activity towards cancer cells, compared to normal human colon tissue cells (CCD 841 CoN cells) ($IC_{50} = 1.15 \pm 0.02$ µM), human fibroblasts ($IC_{50} = 1.21 \pm 0.03$) and PBLs ($IC_{50} = 1.109 \pm 0.13$). In summary, **MM**-compounds exhibited higher activity in cancer cell lines (median $IC_{50} = 0.35$ µM) compared to normal cell lines (median $IC_{50} = 1.11$ µM). We have decided to focus on HT-29 and PC-3 cells in further investigations.

MM-compounds showed higher cytotoxic activity in cancer cell lines than 5-FU used as a reference chemotherapeutic drug. SI calculated as the ratio of median IC_{50} values in normal cell lines and cancer cell lines for **MM**-derivatives equaled 3.17, indicating potential preference of compound's activity in cancer cells.

MitoTracker Red – mitochondrial membrane potential changes ($\Delta\Psi m$)

The change in the MMP results in the deposition of Mitotracker Red reagent in the mitochondrial matrix. The fluorescence intensity reflects the health of the mitochondria and varies with changes in MMP[45].

The fitness of the mitochondria of HT-29 and PC-3 tumor cells was assessed following 24-h treatment of cells with **MM124** and **MM125** in concentrations of 0.5, 1, and 2 µM. A decrease in the fluorescence intensity was observed with an increase in the compounds' concentration (Fig. 3). In the highest concentration of the compound, **MM125** induced the most pronounced decrease in MMP potential in HT-29 (% of control = 78.8 ± 3.32) and PC-3 cell line (% of control = 58 ± 0.58).

Dual acridine orange/ethidium bromide (AO/EB) fluorescent staining

AO/EB fluorescent staining was used to detect apoptosis and necrosis in HT-29 and PC-3 lines exposed to **MM124** and **MM125** compounds (Fig. 4). These cancer cell lines were chosen based on the results of MTT and Mitotracker Red assay. AO/EB staining combines the use of two fluorescent dies that allow distinguishing alive cells (acridine orange stained—green nucleus with red–orange cytoplasm); apoptotic (green irregular nuclei with chromatin condensation or fragmentation) and necrotic cells (ethidium bromide stained—orange

Compound	DLD-1	HT-29	HCT-116	PC-3	BxPC-3	CCD 841 CoN	WI-38	PBLs
	colorectal cancer			prostate cancer	pancreatic cancer	normal human colon tissue cells	normal human fibroblasts	peripheral blood lymphocytes
MM124	0.49 ± 0.04	0.22 ± 0.02	0.38 ± 0.02	0.3	0.32 ± 0.04	1.12 ± 0.04	0.98 ± 0.13	0.87 ± 0.07
MM125	0.55 ± 0.13	0.27 ± 0.02	0.49 ± 0.08	0.43 ± 0.007	0.21 ± 0.02	1.15 ± 0.02	1.21 ± 0.03	1.109 ± 0.13
Median IC_{50} (with interquartile range)	**0.35 µM** (0.26–0.49)					**1.11 µM** (0.95–1.16)		
5-FU	2.68 ± 1.35	4.38 ± 1.1	3.09 ± 0.92	> 360	13.43 ± 1.9	n/d	42.18 ± 7.8	n/d

Table 3. Determination of relative cell viability (IC_{50} values) of cancer cell lines (colorectal cancer (DLD-1, HT-29, HCT-116), prostate cancer (PC-3) and pancreatic cancer (BxPC-3)) or normal cells: normal human colon tissue cells (CCD 841 CoN), human lung fibroblasts (WI-38 cells) and peripheral blood lymphocytes (PBLs), treated with **MM124** and **MM125** using 72-h MTT assay. The values were provided with standard deviation (± SD) [µM]. Additionally, median IC_{50} values obtained for **MM**-compounds in cancer and normal cells were summarized to calculate the selectivity index (SI) (ratio of median IC_{50} values in normal cell lines and cancer cell lines). n/d – non determined

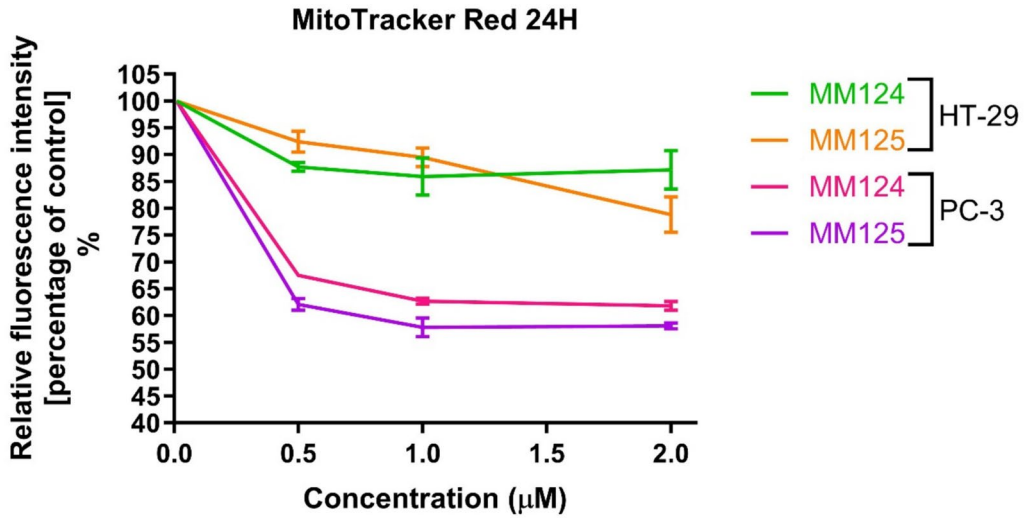

Fig. 3. Changes in the mitochondria membrane potential (MMP) after 24-h incubation with **MM124** and **MM125** in HT-29, and PC-3 cells. Data were presented as a percentage [%] of control cells' fluorescence intensity ± SD value.

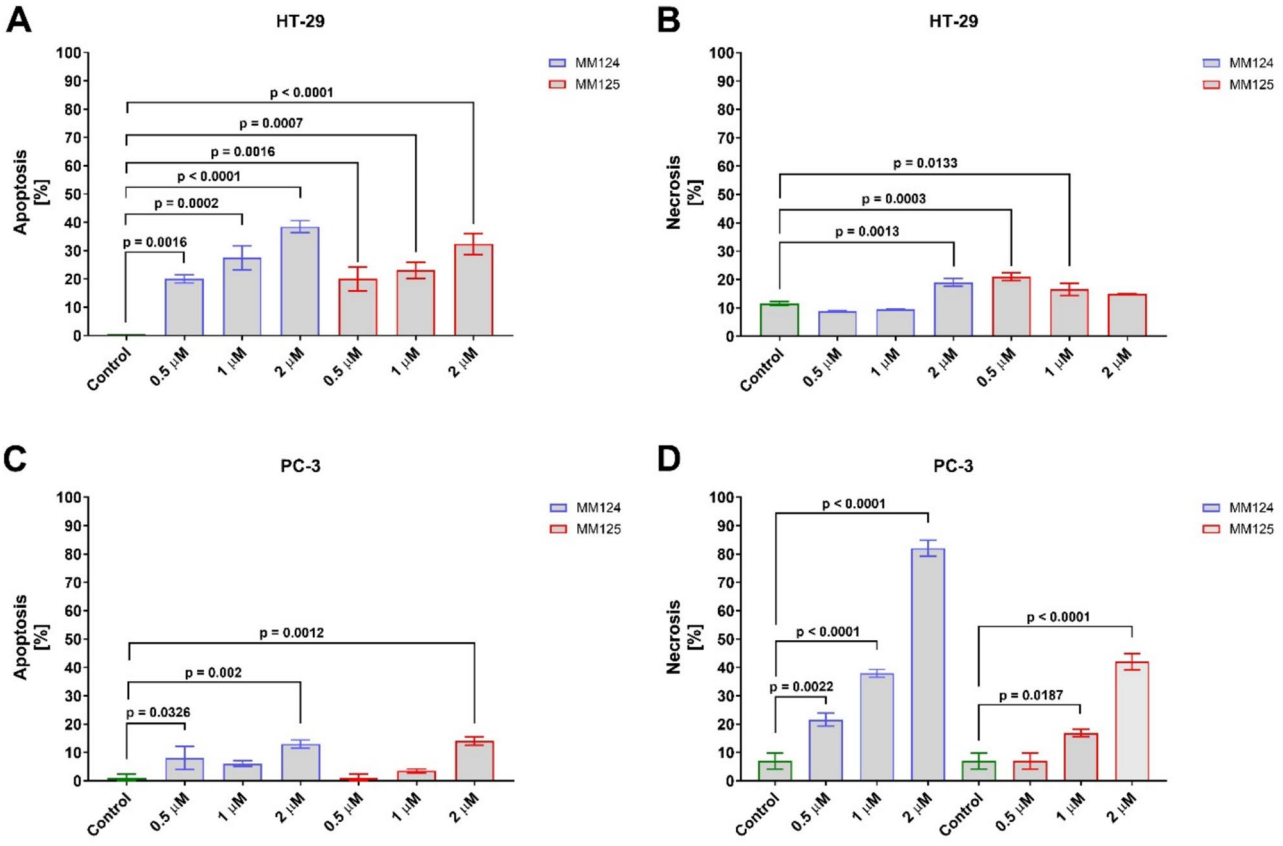

Fig. 4. Determination of apoptosis and necrosis in HT-29 (**A**-**B**) and PC-3 (**C**-**D**) cancer cell lines treated with 0.5, 1, and 2 μM concentrations of **MM124** and **MM125** with AO/EB double staining following 24-h incubation of cells with tested compounds. Data were presented as mean percentage of necrotic and apoptotic cells [%] ± SD values. The differences between the experimental samples and control samples were estimated by the ANOVA test followed by post-hoc Dunnetts's test ($p < 0.05$, $N = 200$).

cell nuclei) upon differential uptake of fluorescent dyes and morphology of cell and chromatin. Apoptosis was observed under a fluorescent microscope and a total of 200 cells were counted [46].

MM124 and **MM125** used in all three tested concentrations (0.5, 1, and 2 μM) induced statistically significant ($p < 0.05$) increase in the % of apoptotic cells in the HT-29 cell line. The number of apoptotic cells increased with an increase in **MM124** and **MM125** concentrations. **MM124** exhibited stronger pro-apoptotic activity in HT-29 cells than **MM125** when used in 1 and 2 μM concentrations. **MM124** induced apoptosis of 27.5 ± 4.24 ($p = 0.0002$) and 38.5 ± 2.12 ($p < 0.0001$) cells after their incubation with 1 and 2 μM concentrations of compound respectively, while the slightly lower pro-apoptotic potential was observed for **MM125** compound (% of apoptotic cells equaled to 23 ± 2.82 ($p = 0.0007$) and 32.35 ± 3.75 ($p < 0.0001$) for incubation of cells with 1 and 2 μM concentrations of the compound respectively) (Fig. 4A). A statistically significant ($p < 0.05$) increase in the necrosis prevalence was observed following 24-h incubation of HT-29 with **MM124** in 2 μM (mean necrosis % = 19 ± 1.41; $p = 0.0013$) concentration and 0.5 (mean necrosis % = 21 ± 1.41; $p = 0.0003$) and 1 μM (mean necrosis % = 16.5 ± 2.12; $p = 0.0133$) concentration of **MM125**. An increase in necrotic cells was observed with the increase in **MM124** concentration. No such effect was observed following incubation with **MM125** (Fig. 4B).

In contrast, in the PC-3 cell line, **MM124** and **MM125** used in the 2 μM concentration induced a statistically significant increase in the number of apoptotic cells (the % of apoptotic cells equaled 13 ± 1.41 ($p = 0.002$) and 14 ± 1.41 ($p = 0.0012$) for **MM124** and **MM125** respectively) (Fig. 4C). Necrosis was the prevalent form of cell death. A statistically significant increase in the number of necrotic cells was observed following 24-h incubation of cells with tested compounds ($p < 0.05$) except from 0.5 μM concentration of **MM125**. **MM124** used in the highest concentrations induced necrosis of 82 ± 2.82 cells ($p < 0.0001$), while **MM125** exhibited lower necrotic potential (% of necrotic cells equalled to 42 ± 2.83; $p < 0.0001$) (Fig. 4D).

Dual propidium iodide/Hoechst 33,342(PI/HE) staining

The rationale for dual labeling with PI/HE is to exploit the contrasting staining characteristics of these dyes to differentiate between viable and dead cells (apoptotic and necrotic) and to observe cell nuclei simultaneously. Functional cells with intact membranes will internalize HE, resulting in a blue fluorescence in their nuclei. However, they will prevent the entry of PI, thus avoiding the emission of red fluorescence from their nuclei. Cells that are dead or have permeabilized membranes will absorb both HE and PI leading to the production of pink fluorescence. Through the analysis of the fluorescence released by the labeled cells using suitable excitation wavelengths, it is feasible to differentiate between living apoptotic and necrotic cells based on their distinct fluorescence characteristics[47].

In the HT-29 cell line **MM124** and **MM125** compounds used in all tested concentrations induced a statistically significant increase in apoptotic cell fraction following 24-h incubation time. **MM124** used in 0.5, 1, and 2 μM concentrations induced apoptosis of 21.5 ± 2.12 ($p = 0.0012$), 32 ± 4.24 ($p < 0.0001$), and 39 ± 5.7% ($p < 0.0001$) of cells respectively, while **MM125** induced apoptosis of 23.5 ± 2.12 ($p = 0.0007$) 25.5 ± 2.12 ($p = 0.0004$) and 37 ± 1.4% ($p < 0.0001$) of cells compared to negative control cells where apoptotic cell fraction was estimated as 0.9 ± 0.28% (Fig. 5A). At the same, **MM124** used in 2 μM (mean necrosis % = 24 ± 1.4; $p = 0.005$) and **MM125** used in 1 μM (mean necrosis % = 21 ± 1.4; $p = 0.0074$) and 2 μM (mean necrosis % = 26.5 ± 0.7; $p < 0.0001$) concentrations induced a statistically significant ($p < 0.05$) increase in necrosis prevalence compared to negative control (mean necrosis % = 16 ± 1.4) (Fig. 5B).

In PC-3 cells, **MM124** used in 0.5 μM (mean apoptosis % = 8.5 ± 2.12; $p = 0{,}0249$), 1 μM (mean apoptosis % = 9.5 ± 0.7; $p = 0.0098$) or 2 μM (mean apoptosis % = 13 ± 1.4; $p = 0.0007$) concentration and **MM125** employed in 1 μM (mean apoptosis % = 9 ± 1.4; $p = 0.0155$) or 2 μM (mean apoptosis % = 17 ± 1.4; $p < 0.0001$) concentrations induced statistically significant ($p < 0.05$) increase in apoptotic cell fraction (Fig. 5C). Similarly to AO/EB staining, the response of prostate cancer cells was directed towards necrosis where **MM124** used in 0.5 μM (mean necrosis % = 21 ± 4.24; $p = 0.0148$), 1 μM (mean necrosis % = 42.5 ± 3.53; $p < 0.0001$) and 2 μM (mean necrosis % = 64.5 ± 6.36; $p < 0.0001$) and **MM125** used in 1 μM (mean necrosis % = 21.5 ± 3.56; $p = 0.0126$) and 2 μM (mean necrosis % = 51 ± 1.4; $p < 0.0001$) induced statistically significant increase in necrotic cell fraction compared to negative control (mean necrosis % = 5.25 ± 0.35) (Fig. 5D).

Study of reactive oxygen species (ROS) formation

Time-dependent change in total cellular ROS levels was analyzed in HT-29 and PC-3 cancer cells by using a DCFH-DA fluorescent probe (Fig. 6)[32,33]. In HT-29 cells **(A)**, the **MM124** compound used in IC_{50} and $2xIC_{50}$ concentrations induced a statistically significant ($p < 0.05$) increase in ROS production following 2-h treatment. ROS generation increased with the rising concentration of **MM**-compound and exceeded levels produced in cells in response to 500 μM H_2O_2. In contrast, the **MM125** compound induced an increase in ROS production when used in the $0.5xIC_{50}$ and IC_{50} concentrations. However, it has not surpassed the ROS-inducing properties of H_2O_2. In PC-3 cells **(B)**, **MM124** used only in $2xIC_{50}$ concentration and **MM125** used in IC_{50} concentration induced a statistically significant increase in ROS production. Nevertheless, ROS levels generated in response to **MM124** used in $2xIC_{50}$ concentration exceeded the ROS formation following H_2O_2 treatment.

Genotoxicity study

DNA damage following 24-h incubation of cells with tested **MM**-compounds was assessed using *OpenComet* software[48] (Fig. 7). Data were presented as % DNA in the comet tail. Mean tail DNA % results recorded for three concentrations (0.5 μM, 1 μM, and 2 μM) of **MM124** and **MM125** were compared to positive and negative controls. **MM**-compounds used in the lowest concentration (0.5 μM) did not induce a statistically significant increase in DNA damage following treatment of both tumor and normal cell lines. In the HT-29 cell line (Fig. 7A), **MM124** used in 1 μM (mean = 28.43 ± 4.77; $p = 0.0004$) and 2 μM (mean = 29.51 ± 2.44; $p = 0.0001$) concentrations and **MM125** used in 2 μM (mean = 24.14 ± 2.83; $p = 0{,}0166$) concentration induced significantly

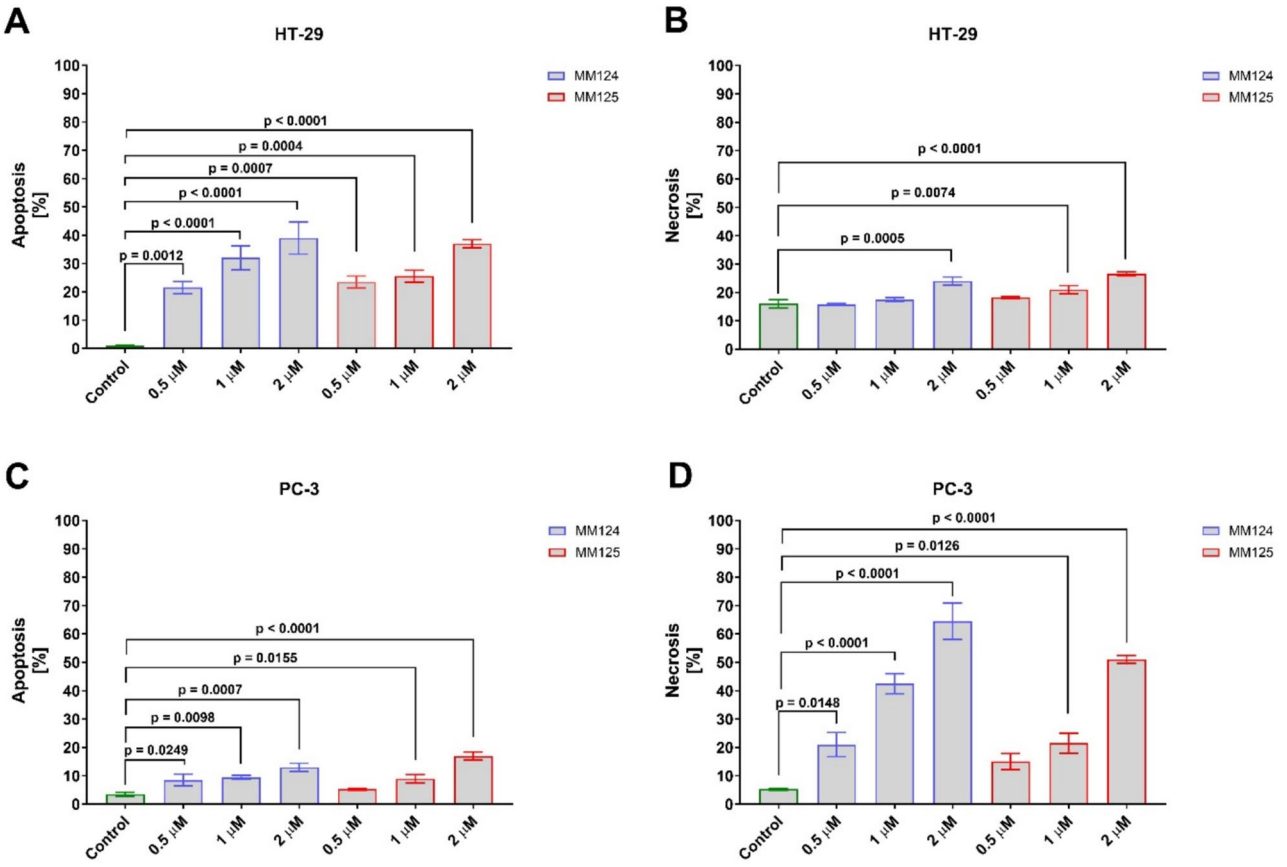

Fig. 5. Determination of apoptosis and necrosis in HT-29 (**A**-**B**) and PC-3 (**C**-**D**) cancer cell lines treated with 0.5, 1, and 2 μM concentrations of **MM124** and **MM125** with PI/HE double staining following 24-h incubation of cells with tested compounds. Data were presented as mean percentage of necrotic and apoptotic cells ± SD values. The differences between the experimental samples and control samples were estimated by the ANOVA test followed by post-hoc Dunnetts's test ($p < 0.05$, $N = 200$).

higher increase in DNA damage compared to negative control. However, DNA damage has not exceeded the one induced by positive control (20 μM bleomycin; mean = 33.58 ± 3.62; $p < 0.0001$). DNA damage induced by **MM124** and **MM125** in all tested concentrations was substantially higher in the PC-3 cancer cell line (Fig. 7B) compared to PBL_S (Fig. 7C). A statistically significant ($p < 0.05$) increase in DNA damage was observed for the 1 and 2 μM concentrations of **MM124** ($mean_{1\mu M} = 49.52 \pm 4.28$; $mean_{2\mu M} = 56.5 \pm 6.65$; $p < 0.0001$) and **MM125** ($mean_{1\mu M} = 38.8 \pm 4.36$; $mean_{2\mu M} = 57.99 \pm 6.96$; $p < 0.0001$) in PC3 cells compared to the negative control (Fig. 7B). The DNA damage induced by the compounds used in the highest concentration has exceeded the levels induced by 20 μM bleomycin (mean = 44.99 ± 2.37; $p < 0.0001$). In PBLs (Fig. 7C), **MM124** used in 1 μM (mean = 13.08 ± 0.86; $p < 0,0001$) concentration, and **MM125** used in 1 μM (mean = 15.4 ± 1.8; $p = 0.0319$) and 2 μM (mean = 27.76 ± 3.12; $p < 0.0001$) concentrations induced statistically significant increase in DNA compared to negative control. The levels of DNA damage have not exceeded the ones induced by positive control (mean = 41.33 ± 1.95; $p < 0.0001$). DNA damage induced by **MM124** and **MM125** increased with the increase in their concentration – a dose–response relationship was observed in all cell lines. Examples of comets obtained in the experiment in the HT-29 and PC-3 cell lines were shown in Figs. 8 and 9 respectively.

Electrochemical studies

The electrochemical characteristics of **MM124** and **MM125** were examined under physiological pH conditions, for a better understanding of the occurring DNA interaction with the chosen sulfonamide derivatives. In the preliminary experiments performed using SW voltammetry, both, oxidation and reduction of the sulfonamides were observed. Figure 10A shows the SW voltammograms of **MM124** and **MM125** recorded within the potential window from 0 to – 0.5 V, for the same concentrations of the compounds. As can be seen, **MM124** and **MM125** exhibited one reduction and one oxidation peak, both ca. – 0.265 V vs. Ag/AgCl, in the applied potential range. For both compounds, the observed reduction signals were significantly higher than those caused by compound oxidation. Sequential studies were conducted using cyclic voltammetry. Interestingly, for both compounds, only signals originating from analytes reduction were observed (see Fig. 10B) despite changes in the direction of the potential sweep. Based on the obtained results, it can be clearly stated how significantly the scan rate affects the kinetics of the electrode processes.

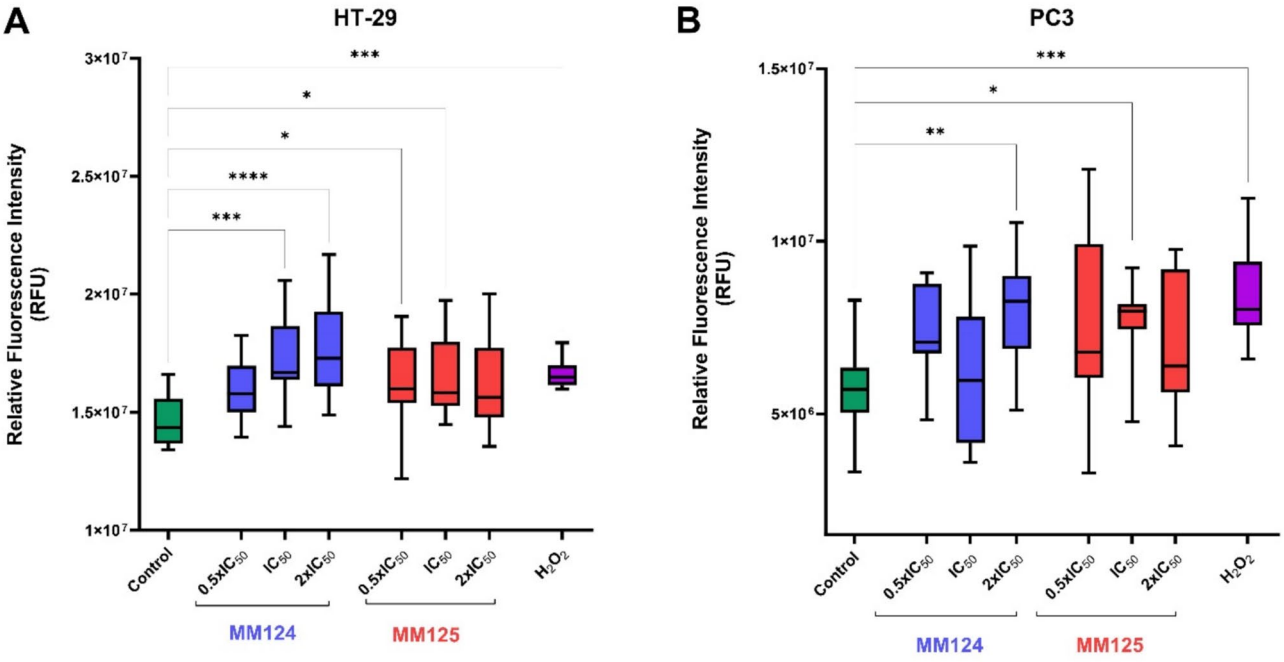

Fig. 6. Reactive oxygen species (ROS) generation in HT-29 (**A**) and PC-3 (**B**) cells after 2-h treatment with **MM124** and **MM125** at concentrations of 0.5xIC_{50}, IC_{50}, and 2xIC_{50} concentrations and 500 µM H_2O_2 used in the experiment as a positive control. Data were presented as median relative fluorescence intensity units (RFU) with interquartile range and minimal and maximal values. The Kruskal–Wallis test was employed to show a statistically significant difference between groups. Dunn's multiple comparisons test was used to compare mean rank differences between control and treated groups. In all groups, $N = 15$. Significant changes: * $p < 0.05$; ** $p < 0.01$, ***; $p < 0.001$; $p < 0.0001$.

To evaluate whether the mass transfer of **MM124** and **MM125** toward the BDD electrode surface was controlled by adsorption or diffusion, the effect of various scan rates on chosen sulfonamide derivatives signals was investigated. The CV curves of **MM124** and **MM125** recorded within the potential window ranging from – 0.7 to 0.2 V at various scan rates are presented in Fig. 10B. It is worth noting that the surface of the BDD electrode, used in the present study, exhibits relatively low adsorption properties, suggesting that diffusion-controlled processes were expected[49]. The linear dependence between the peak current (I_p) of both **MM124** and **MM125** and the square root of the scan rate ($\nu^{1/2}$) were determined, demonstrating that diffusion played a crucial role in the electrode reaction of chosen sulfonamides. Additionally, the plots of log I_p *vs.* log ν yielded straight lines with slopes of 0.47 for **MM124** and 0.45 for **MM125,** which are close to the theoretical value of 0.5[50], typically observed for diffusion characteristics of the registered currents.

The interaction of **MM124** and **MM125** with dsDNA was investigated using the SWV technique. The addition of dsDNA to the sulfonamides solutions significantly decreased the peak currents of both analytes (See Fig. 11). It is worth mentioning, that dsDNA was also analyzed separately in the same experimental conditions and neither anodic nor cathodic peaks were observed (data not shown). Therefore, it can be concluded that the observed decreases in the peak currents of **MM124** and **MM125** in the presence of dsDNA are likely due to the binding of the analytes to the large, slowly diffusing dsDNA, resulting in a significant decrease in the diffusion coefficient value.

During the evaluation of DNA interaction with the selected sulfonamides, no notable shifts in peak potentials were detected. Since a shift in peak potential is typically associated with intercalative interactions, we can likely exclude this type of interaction between **MM124** /**MM125** and dsDNA. Additionally, during the voltammetric analyses, interaction studies were conducted by incubation of the analyzed compounds with dsDNA for a specified period. However, no significant differences in the obtained signals were observed as a result of the incubation of these compounds.

In summary, considering the observed significant decrease in current values of **MM124** and **MM125** in the presence of increasing amounts of dsDNA, it can be concluded that interactions occur between dsDNA and the selected sulfonamides. However, these studies indicate the DNA interaction other than the intercalative type typical for hydrophobic and planar compounds like the tested sulfonamides.

Computational analysis

Drug likeness and ADMET

ADMET properties and drug-likeness prediction for the designed compounds—**MM124** and **MM125** have revealed that both compounds follow Lipinski's rule of five with one common violation related to the number

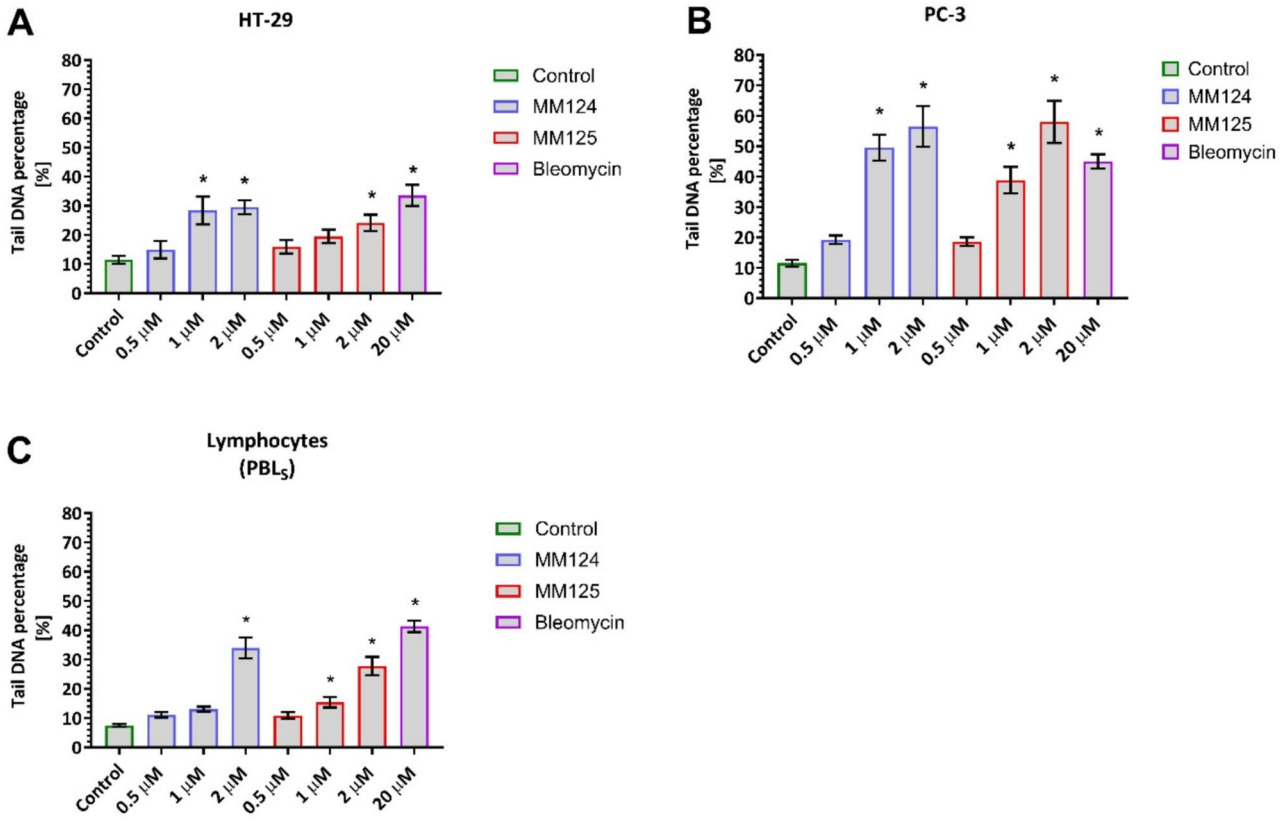

Fig. 7. DNA damage induced by 0.5 µM,1 µM, and 2 µM concentrations of **MM124** and **MM125** in cancer cell lines (HT-29 (**B**), PC-3 (**C**)) and PBLs (**D**). Data were represented as mean tail DNA % with ± SEM values. The differences between the experimental samples and control samples were estimated by the ANOVA test followed by post-hoc Dunnett's test ($p < 0.05$, $N = 200$). * significant difference compared to the negative control (untreated cells).

of hydrogen bond acceptors. The obtained physicochemical properties for both the designed compounds as per Lipinski's rule of five were tabulated in Table 4.

The ADMET properties of both the designed compounds **MM124** and **MM125** related to their BBB permeability, GI absorption, hepatotoxicity, cardiotoxicity, and CYP inhibition predicted by pkCSM[39], SwissADME[40], and PreADMET online server were summarized in Table 5.

The presence of other major toxic effects like immunotoxicity, mutagenicity, etc. for both the designed molecules **MM124** and **MM125** were additionally predicted by using the Protox-II webserver was tabulated in Table 6.

MM124 and **MM125** compounds may exhibit low oral bioavailability due to the low GI absorption. Also, their activity in the brain compartment may be limited because of no BBB permeability and the fact that both compounds may act as P-glycoprotein substrate (P-gp) substrates. The BBB is composed of endothelial cells of capillaries that protect the brain cells from potentially toxic compounds. P-gp is an ATP-dependent drug transport protein located mostly in the apical membranes of several epithelial cell types that actively transport agents out of the cell[51].

Human cytochrome CYP P450 enzymes are extensively involved in drug detoxification, cellular metabolism, and homeostasis. Members of the cytochrome CYP P450 family are responsible for almost 80% of oxidative metabolism and roughly 50% of the overall elimination of major pharmaceutical agents in humans. CYPs can modify drug responses in many ways, including their influence on drug elimination, action, safety, bioavailability, and drug resistance[52]. **MM124** compound may not inhibit the activity of major drug-metabolizing CYP enzyme isoforms CYP2D6 and CYP3A4, while the effect of **MM125** on CYP3A4 inhibition seems to be ambiguous.

One of the leading reasons for new drug withdrawal from a clinical setting is drug-induced hepatotoxicity which can lead to liver failure[53]. According to the in silico predictions performed for **MM124** and **MM125** the toxic effect of compounds on the liver cells is unclear. According to the Swiss-ADME webserver, both compounds may exhibit hepatotoxic activity. However, the Protox-II server classifies compounds as inactive for hepatotoxicity endpoint. Nonetheless, the probability of this prediction is low ($p = 0.55$).

The ability of laboratories to test compounds for mutagenicity was substantially improved after Bruce Ames created and published a bacterial strain and a mutagenicity assay in 1973. The now-famous "Ames Test" required little training, could be completed in two days, and demanded little equipment could be quickly and reliably replicated in different labs. The Ames test is still widely used in commercial chemical testing, despite

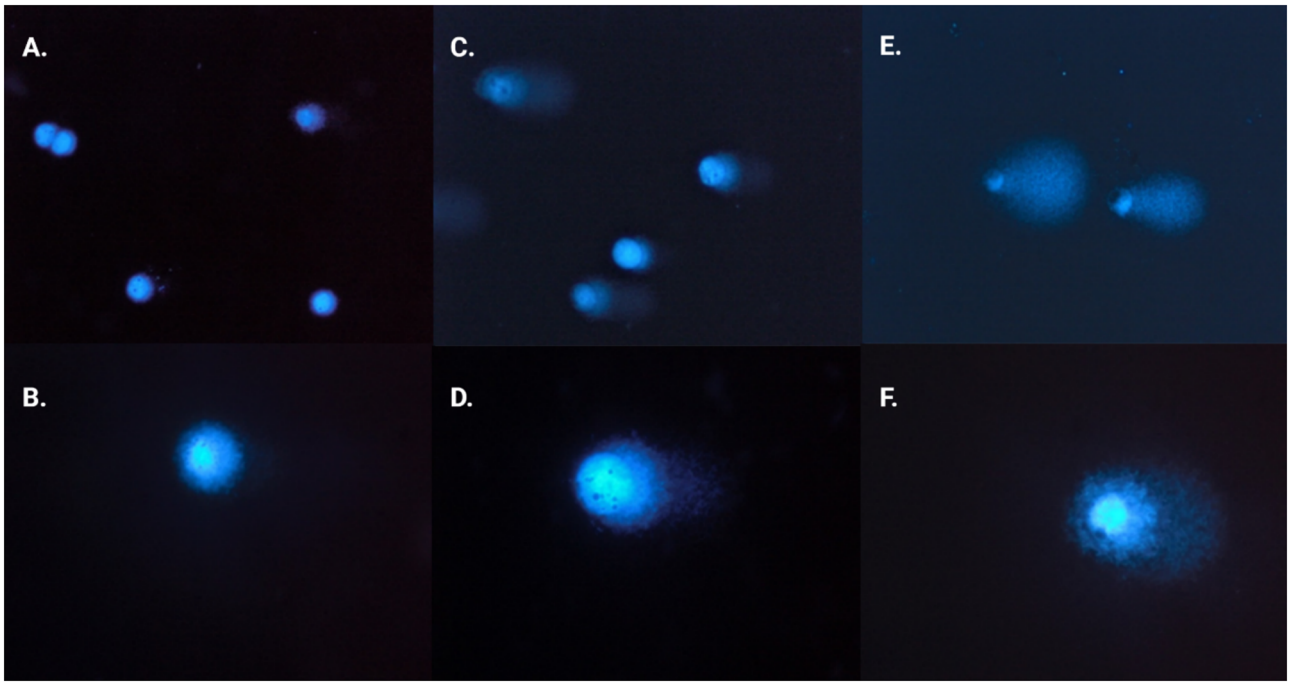

Fig. 8. Images of comets obtained in an alkaline comet assay. Control samples (**A** and **B**), 2 µM **MM125** (**C** and **D**), and 20 µM bleomycin (**E** and **F**) in the HT-29 cell line. Upper images are shown in magnification of 200X. Lower images are shown in magnification 400X.

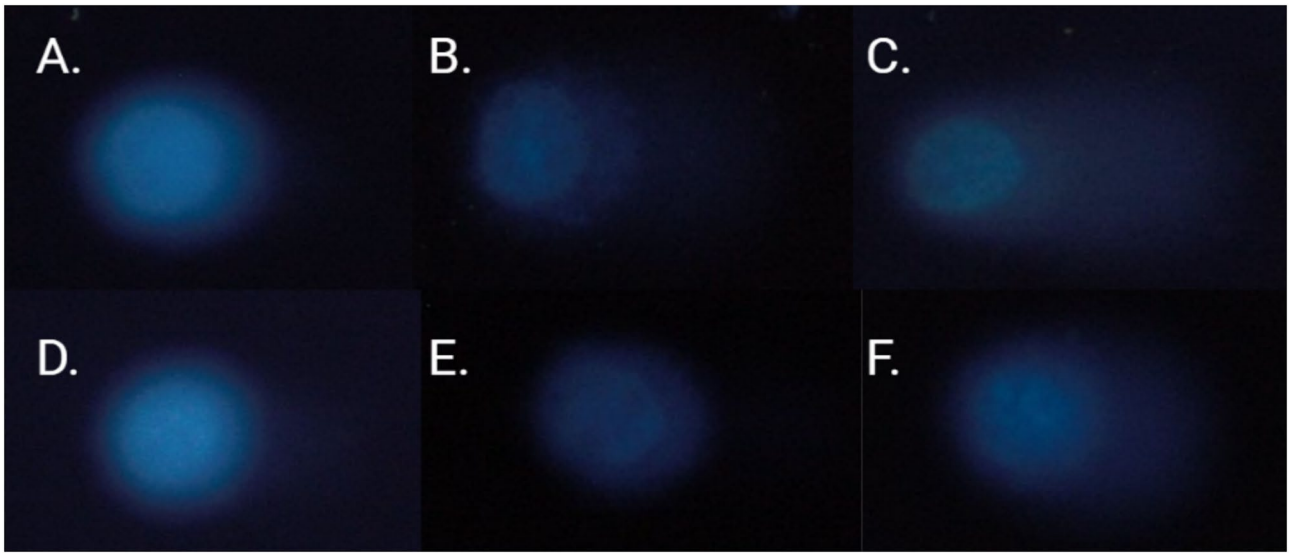

Fig. 9. Increase in DNA damage following treatment of PC3 cells with three tested concentrations (0.5, 1, and 2 µM) of **MM124** (**A**-**C**) and **MM125** (**D**-**F**). Images were shown in magnification of 400X.

the discovery of other methods to evaluate the mutational properties of compounds. Investigated in this study **MM**-compounds were found to lack the mutagenic properties by all the softwares/servers used in the in silico predictions[54].

Cardiotoxicity constitutes an important side-effect associated with the used of many commonly used drugs. In the majority of cases, it results from the interaction with the potassium ion channel of the human ether-a-go-go-related gene (hERG). The inhibition of hERG causes long QT syndrome (LQTS), a potentially fatal heart condition. The elimination of potentially harmful drug candidates through the use of a virtual screening method to anticipate drug-induced hERG-related cardiotoxicity is important for the drug discovery process[55].

The investigation revealed the effect of **MM124** and **MM125** compounds on hERG inhibition is ambiguous. Among other toxicological endpoints, it is important to evaluate the toxic effect of compounds on the immune

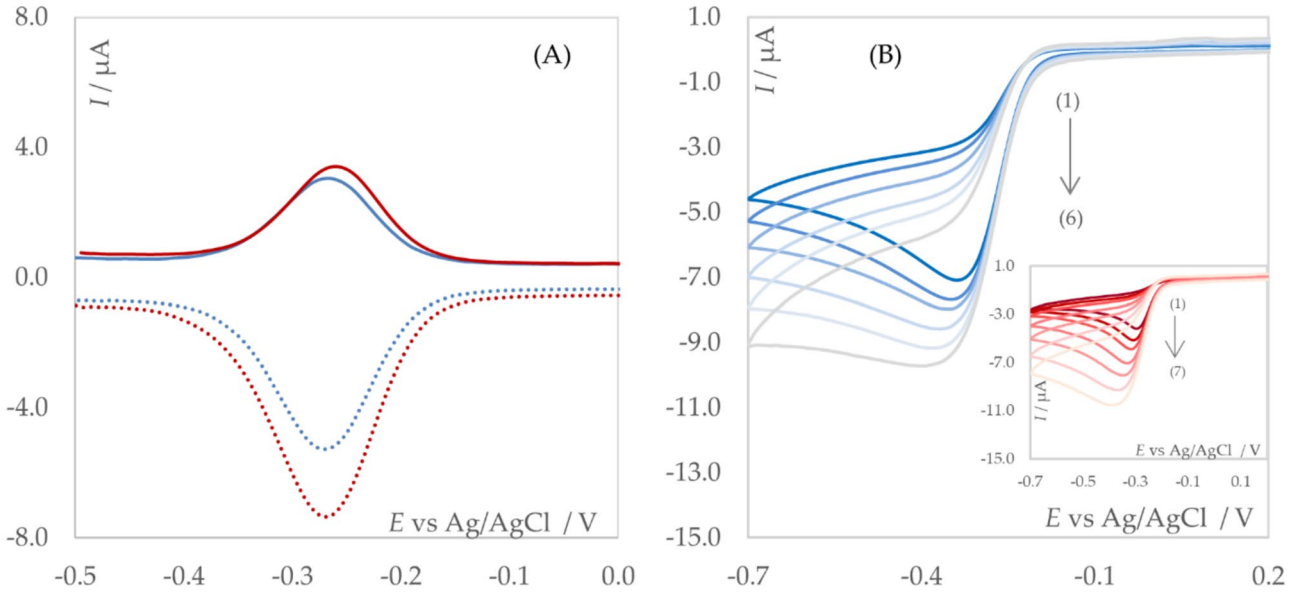

Fig. 10. (**A**) SW voltammograms of **MM124** (blue lines) and **MM125** (red lines) for anodic (solid lines) and cathodic (dotted lines) direction of the potential sweep, $c(_{\mathbf{MM125}}) = c(_{\mathbf{MM124}}) = 1.0 \times 10^{-4}$ mol L^{-1}; supporting electrolyte: PBS pH 7.4; (**B**) Cyclic voltammogram of **MM124** (main plot) and **MM125** (inset) recorded at various scan rates of 50 (1), 75 (2), 100 (3), 200 (4), 300 (5), 400 (6), 500 (7) mV s^{-1}, $c(_{\mathbf{MM125}}) = c(_{\mathbf{MM124}}) = 1.0 \times 10^{-4}$ mol L^{-1}; supporting electrolyte: PBS pH 7.4.

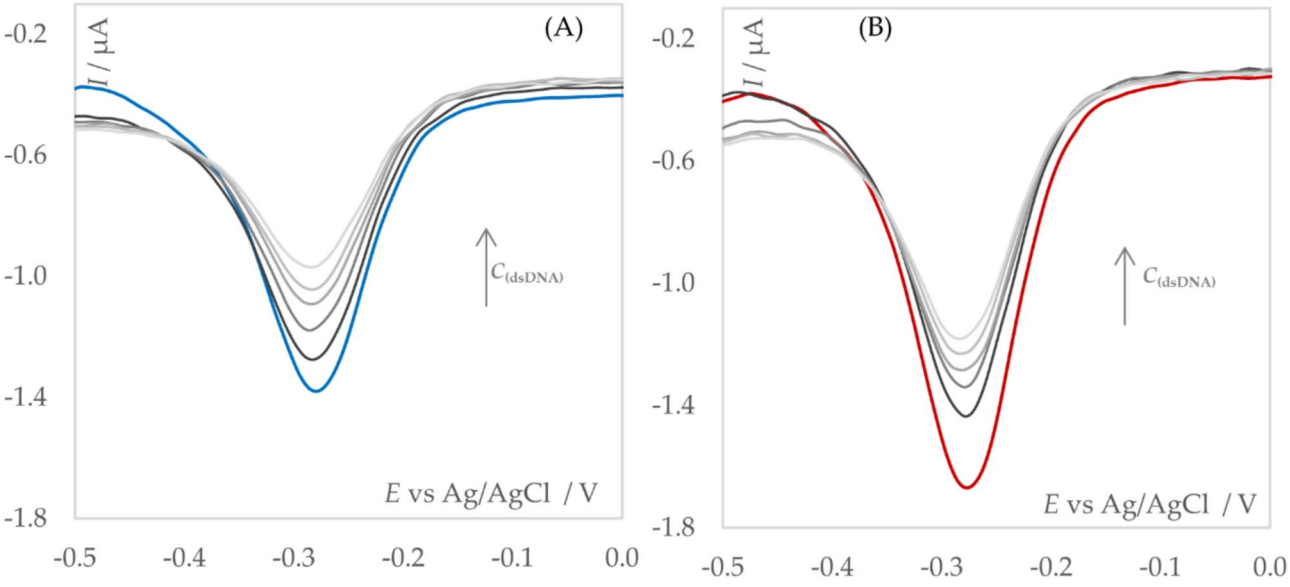

Fig. 11. (**A**) SW voltammograms of **MM124** (blue line) recorded with progressively increasing amounts of dsDNA (gray lines), $c(_{\mathbf{MM124}}) = 1.0 \times 10^{-5}$ mol L^{-1}, $c(_{\mathrm{dsDNA}}) = 10 - 50$ mg L^{-1}; (**B**) SW voltammograms of **MM125** (red line) recorded with progressively increasing amounts of dsDNA (gray lines), $c(_{\mathbf{MM125}}) = 1.0 \times 10^{-5}$ mol L^{-1}, $c(_{\mathrm{dsDNA}}) = 10 - 50$ mg L^{-1};

Compound	Molecular weight	Hydrogen bond acceptors	Hydrogen bond donors	Consensus Log P value	Lipinski violations
MM124	431.47 g/mol	10	2	1.23	Yes; 1 violation: NorO > 10
MM125	431.47 g/mol	10	2	1.17	Yes; 1 violation: NorO > 10

Table 4. Predicted molecular properties describing Lipinski's rule of five.

Compound /Property	Gastrointestinal (GI) absorption	CYP2D6 inhibitor	CYP3A4 inhibitor	Blood Brain Barrier (BBB) permeability	P-glycoprotein substrate	Ames Toxicity	Cardiotoxicity (hERG inhibition)	Hepatotoxicity
MM124	Low	No	No	No	Yes	No	Ambiguous	Yes
MM125	Low	No	No/Yes	No	Yes	No	Ambiguous	Yes

Table 5. Predicted ADMET properties of **MM124** and **MM125**.

Compound /Property with probability	Hepatotoxicity	Immunotoxicity	Mutagenicity
MM124	Inactive (p = 0.55)	Inactive (p = 0.99)	Inactive (p = 0.66)
MM125	Inactive (p = 0.55)	Inactive (p = 0.99)	Inactive (p = 0.66)

Table 6. Toxicity profiles of **MM124** and **MM125** estimated using Protox-II (http://tox.charite.de/protox_II).

system. Immunotoxicity of the drugs is a leading cause of morbidity and mortality in patients undergoing treatments. The most common immunotoxic consequence of medicines include hypersensitivity (allergic and anaphylactic) reactions[56]. According to the in silico predictions **MM124** and **MM125** with high probability may not exert immunotoxic effects.

Molecular docking

The map files for various atom types of the macromolecular target as well as ligands generated by the Autogrid utility were used in the Autodock software to perform molecular docking simulations. The docking protocols for the concerned macromolecular targets used in the current study were successfully validated by considering the binding energy, overlay conformation, and chemical resemblance based on the observed chemical interactions of the docked conformation of the reference ligand ellipticine with reference to its bioactive conformation. The overlaid conformation (a) and chemical interactions (b) of the docked conformation of the reference ligand ellipitiicne was represented in Fig. 12.

After validation of molecular docking, we have employed the above-stated parameters to run the simulation studies of **MM124** and **MM125** chiral sulfonamides, and the observed docking results were provided in Table 7.

The two-dimensional binding interactions and three-dimensional binding conformation of **MM124** and **MM125** with DNA were represented in Fig. 13 and Fig. 14 respectively.

Based on the observed binding energy and type of the interacting residues it can be concluded that compounds exhibit a similar binding pattern as ellipticine used in our study as a reference compound.

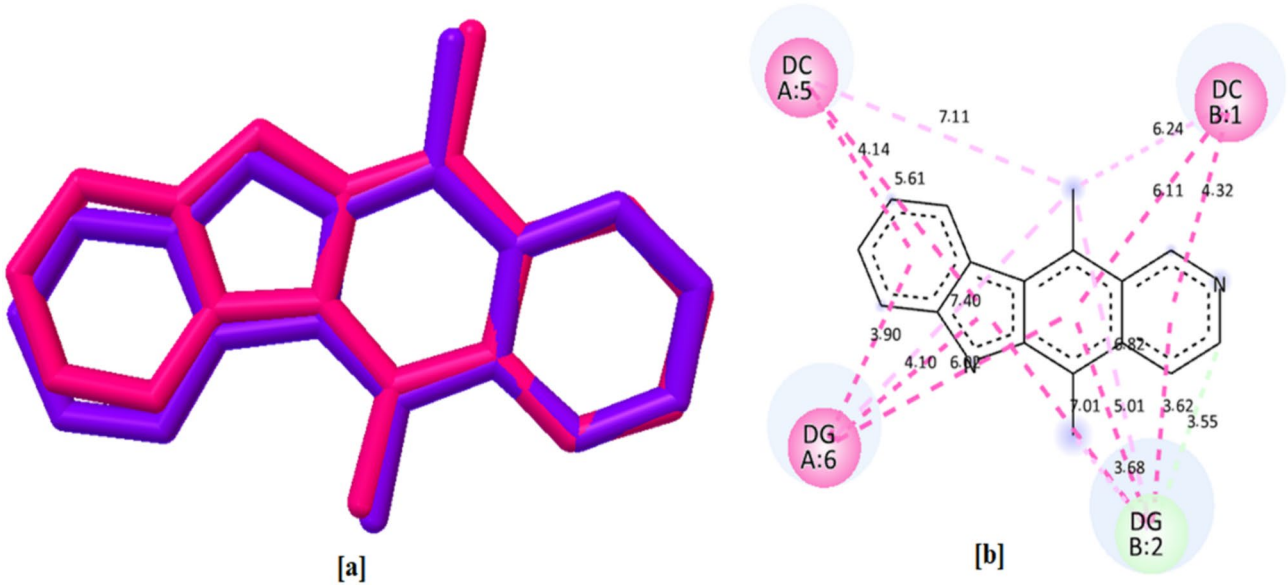

Fig. 12. Overlaid conformation (**a**) and chemical interactions (**b**) of the docked conformation of the reference ligand ellipiticine.

Ligand	Binding energy (kcal/mol) (PDB: 1z3f.)	Interacting residues
MM124	-7.59	DC_A5, DG_A6, DC_B1, DG_B2, DA_B3
MM125	-8.18	DC_A5, DG_A6, DC_B1, DG_B2
Ellipticine (reference ligand)	-8.75	DC_A5, DG_A6, DC_B1, DG_B2

Table 7. Binding energy (kcal/mol) obtained after performing a docking analysis of both the designed molecules (**MM124**, **MM125)** and the standard inhibitor ellipticine complexed in the studied PDB structure (PDBid:1Z3F).

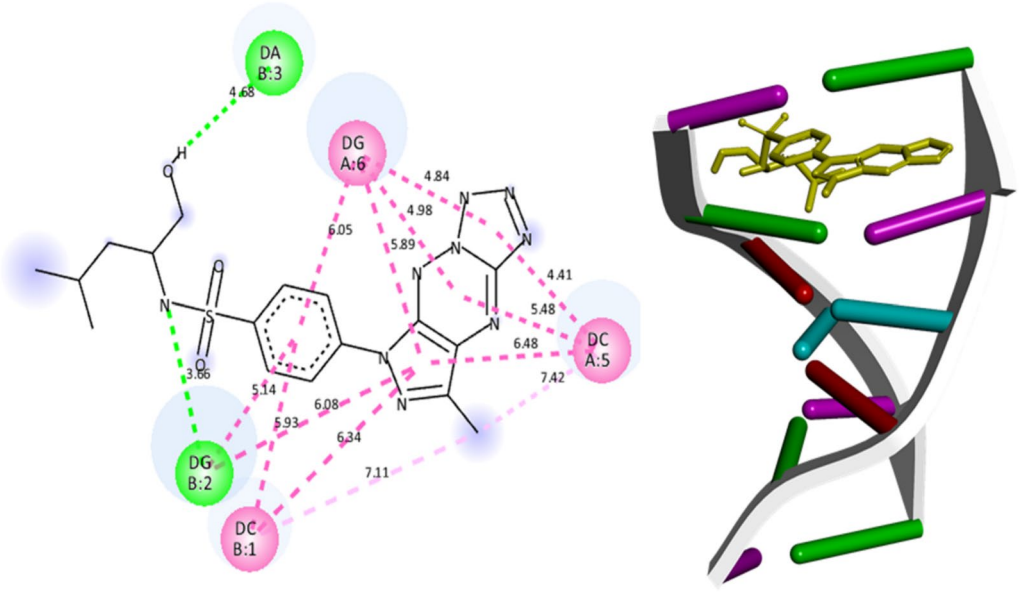

Fig. 13. Two-dimensional binding interactions and three-dimensional binding conformation of **MM124** with DNA molecule.

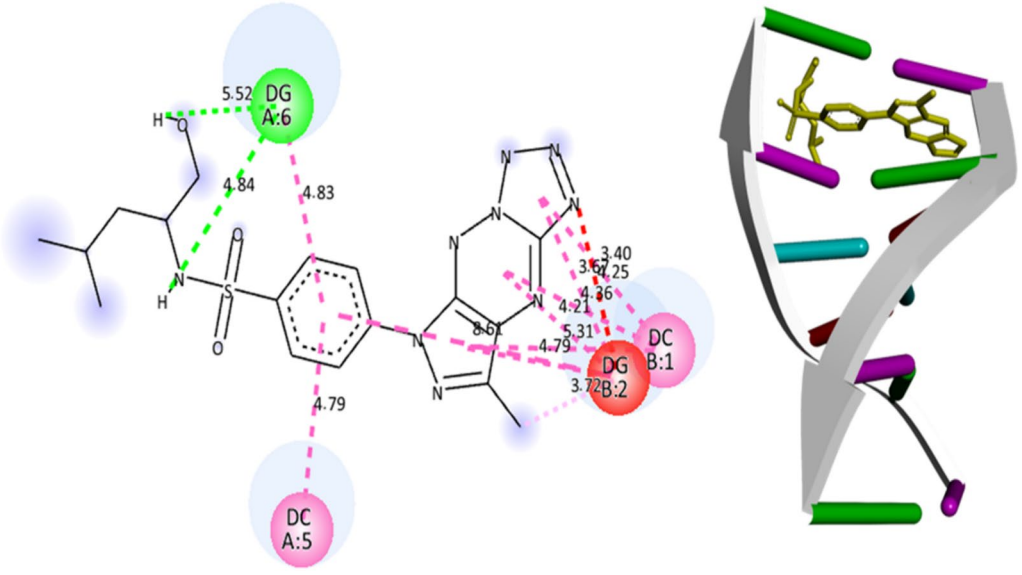

Fig. 14. Two-dimensional binding interactions and three-dimensional binding conformation of **MM125** with DNA molecule.

Molecular dynamics simulation

The molecular dynamics (MD) simulation of the ligand **MM125** in complex with DNA revealed several key insights into its flexibility, stability, and dynamic behavior. **MM125** was found to possess eight flexible bonds involving 30 heavy atoms out of a total of 54 atoms. The flexibility of individual atoms or residues in the ligand or macromolecular structure was assessed through the root-mean-square fluctuation (RMSF). RMSF is a critical parameter that provides insights into the dynamic behavior and relative flexibility of the macromolecular complex. The RMSF values for the ligand during the simulation ranged from 0.5 to 3.5 Å, indicating relative flexibility within the binding site. The structural stability of the ligand within the DNA binding cavity was analyzed using the root-mean-square deviation (RMSD). During the simulation period, the ligand exhibited RMSD values within the range of 1.5–2.4 Å, demonstrating minimal fluctuations. The overall RMSD analysis confirmed that the **MM125**-DNA complex maintained a high degree of thermodynamic stability with only minor deviations from the initial position throughout the simulation. The radius of gyration (rGyr) was calculated to evaluate the compactness and conformational stability of the complexed ligand. The rGyr values for **MM125** complexed with DNA were observed within the range of 4.0–5.0 Å, further confirming good conformational stability during the simulation. Overall, the MD simulation of the **MM125**-DNA complex over 100 ns concluded that the ligand displayed stable binding within the target DNA's active site, with limited fluctuations and consistent conformational behavior. The RMSD (1.5–2.4 Å), RMSF (0.5–3.5 Å), and rGyr (4.0–5.0 Å) collectively highlight the robust interaction and stability of the complex. The RMSD **(a)**, rGyr **(b),** and RMSF **(c)** for **MM125** complexed with DNA throughout the 100 ns MD simulation was represented in Fig. 15.

In summary, docking analysis of **MM124**, and **MM125** compounds against 6-BP DNA molecule to predict their intercalation property has revealed that both the compounds **MM125** and **MM124** are showing good binding affinity against the DNA similar to that of the reported standard intercalating ligand ellipticine. Although both the concerned compounds **MM125** and **MM124** are showing worse binding interactions with DNA when compared with the reference compound ellipticine. MD simulation of the compound **MM125** has revealed that the ligand is sufficiently stabilized within the macromolecular cavity of DNA to impart the biological effect.

Discussion

Common methods of cancer treatment include radiotherapy, gene therapy, hormone therapy, immunotherapy, and surgery. Until now, the most popular therapeutic option is chemotherapy, based on the use of cytostatic drugs that cause damage to the genetic material of cancer cells. Due to the mechanism of action, cytostatics are divided into (a) alkylating agents that inhibit the ability of cells to replicate DNA (cyclophosphamide, cisplatin, carboplatin); (b) antimetabolites which disrupt the biosynthesis of nucleic acids (5-FU), gemcitabine, 6-mercaptopurine); (c) plant alkaloids, including topoisomerase inhibitors (topotecan, irinotecan) and taxols, causing abnormal mitotic spindle formation (docetaxel, paclitaxel), (d) anti-cancer antibiotics that disrupt the double-helix sugar-phosphate backbone (mitomycin C and other bleomycin)[57,58]. The treatment process is selected individually and may involve both the combination of various therapeutic methods and various cytostatic agents. The effectiveness of multi-drug programs is based mainly on the synergistic effect of substances that surpass the effects of monotherapy[59].

The most common cause of chemotherapy failure is the emergence and development of multidrug resistance, defined as increased insensitivity of cancer cells to the therapeutic agents. This phenomenon may have a genetic

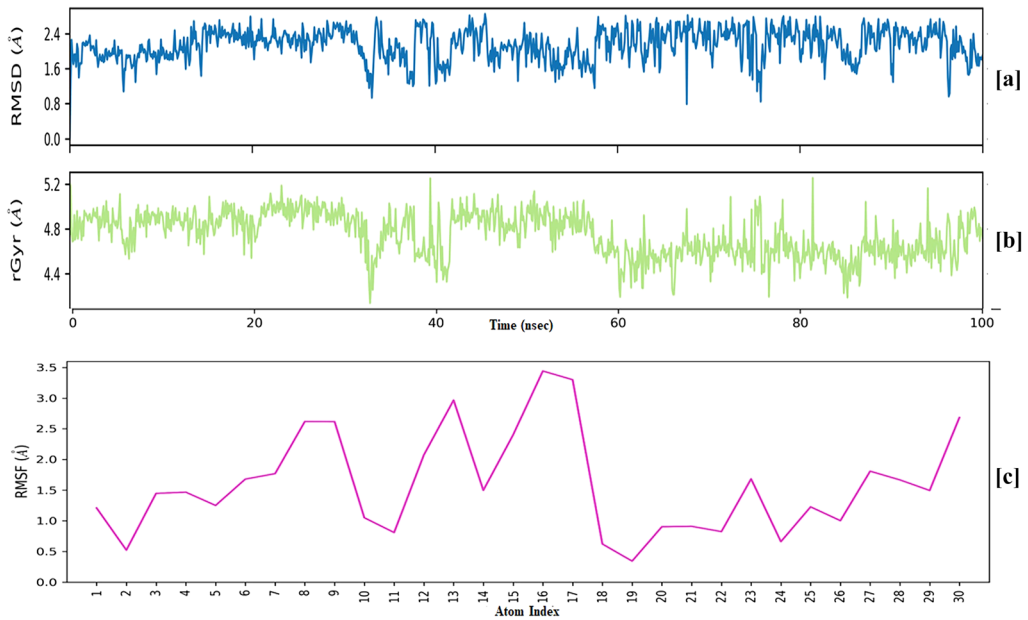

Fig. 15. The root-mean-square deviation (RMSD) (**a**), radius of gyration (rGyr) (**b**) and root-mean-square fluctuation (RMSF) (**c**) for MM125 complexed with DNA throughout the 100 ns MD simulation.

basis or be associated with an increased outflow of chemotherapeutic agents, intensification of repair processes in cancer cells, deregulation of apoptotic pathways, or reduced affinity for drugs[58,60]. Attempts to overcome drug resistance focus on understanding the biological basis of multidrug resistance development and the use of combination therapies with low-toxicity pharmaceuticals targeting imperfections in cellular mechanisms. The complicated nature and heterogeneity of neoplastic diseases are the main reasons for the growing need to search for new oncotherapeutic agents with selective action and safety profiles. Identification of substances that increase the effectiveness of existing drugs, or allow to bypass of the multidrug resistance phenomenon, brings hope to patients with the worst prognosis[58].

Heterocyclic compounds, especially those with nitrogen atoms are the cornerstone of pharmaceutical agents, antibiotics, and agrochemicals. Approximately 75% of FDA-approved drugs contain a nitrogen heterocycle, underscoring their importance in medicinal chemistry. Among these, 1,2,4-triazine derivatives are particularly noteworthy given their anticancer potential. For instance, avapritinib, a kinase inhibitor of platelet-derived growth factor receptor α (PDGFRα), was approved in 2020 for treating gastrointestinal stromal tumors. Its efficacy has prompted further clinical trials for treating other advanced solid tumors, such as lung, breast, melanoma, and sarcoma[61].

A promising strategy in chemotherapeutic development involves combining fragments of known drugs into a single molecule to enhance biological activity. The natural pyrazolo[4,3-*e*][1,2,4]triazine system, when combined with pharmacophore groups, offers opportunities to design new compounds with potential anticancer properties[24,62]. Studies have shown that pyrazolo[4,3-*e*][1,2,4]triazine derivatives exhibit moderate antitumor activity. For instance, aza-sildenafil analogs and aniline-substituted pyrazolo[4,3-*e*][1,2,4]triazine sulfonamides have demonstrated effectiveness against cancer cells. Modifying the pyrazolo[4,3-*e*][1,2,4]triazine structure by incorporating tetrazole or triazole rings has also been shown to increase cytotoxic activity against cancer cell lines. These modifications highlight the potential of structural adjustments in enhancing the efficacy of pyrazolo[4,3-*e*][1,2,4]triazine derivatives as recently reviewed[7].

The combination of pyrazolo[4,3-*e*][1,2,4]triazine with tetrazole ring, sulfonamide moiety, and leucinol represents a promising chemical structure in cancer treatment. Incorporating leucinol in the chemical structure of the compound can offer several advantages for the development of potential drug-like molecules. First of all, the lipophilic side chain of leucinol can affect membrane permeability, helping the compound enter cells more efficiently. Leucinol can also mimic leucine residues in biological systems and can be used in peptidomimetic design. This allows interaction with amino acid-binding sites on enzymes, transporters, or receptors. Furthermore, cancer cells often overexpress L-type amino acid transporters (LAT1, etc.) to support rapid growth. Compounds incorporating amino acid-like moieties (like leucinol) may exploit these transporters for selective uptake by cancer cells. Adding leucinol can also impact water solubility, reduce metabolic degradation, or enhance plasma stability depending on the context making it useful for successful drug design[63–68].

The chirality of drug molecules can significantly influence their pharmacological activity. Research has demonstrated that different enantiomers of a compound can exhibit varying degrees of therapeutic efficacy and side effects. In studies on pyrazolo[4,3-*e*][1,2,4]triazine derivatives, it was observed that R-enantiomers generally exhibit slightly higher cytotoxic activity compared to their S-isomers[61]. Therefore, we aimed to investigated two enantiomeric pyrazolo[4,3-*e*][1,2,4]triazine leucinol derivatives **MM124** (R-enantiomer) and **MM125** (S-enantiomer).

The present study confirmed high, micromolar cytotoxicity (median $IC_{50} = 0.35$ μM) of the **MM124** and **MM125** compounds towards cancer cell lines of different origins including colorectal (DLD-1, HCT-116, HT-29), pancreatic (BxPC-3) and prostate (PC-3) cancer with minor effect on normal human colon tissue cells (CCD 841 CoN), fibroblasts (WI-38) and peripheral blood lymphocytes (PBLs) in vitro. Although **MM124** (R-enantiomer) exhibited slightly greater cytotoxic potency compared to **MM125** (S-enantiomer), the difference was not sufficient to establish a clear structure–activity relationship. Importantly, both **MM**-compounds outperformed the standard chemotherapeutic agent 5-fluorouracil (5-FU) in terms of overall cytotoxic efficacy. However, 5-FU displayed superior selectivity toward malignant cells over normal cells.

It was also found that tested compounds induced oxidative stress and apoptosis of colorectal (HT-29) and prostate (PC-3) cancer cells as evidenced by the loss of MMP and features characteristic for apoptosis evidenced by dual fluorescent staining techniques. Nevertheless, the response of PC-3 cells seemed directed more to the necrotic type of cell death, which may lead to undesirable side effects. This is consistent with our previous studies where other pyrazolo[4,3-*e*][1,2,4]triazine sulfonamide compounds fused with tetrazole ring also induced necrotic response in PC-3 cells rather than apoptotic response compared to pancreatic BxPC-3. This may indicate the complex response of cancer cells to **MM**-compounds[24].

We have also found that the genotoxic effect exhibited by the compounds may be the direct consequence of the ongoing cell death process or may be the underlying cause of the high cytotoxicity exhibited by the compounds. This observation is also consistent with our previous findings for other compounds of the same class[23,69] and is common for other anti-cancer agents used in clinical practice like bleomycin used in our genotoxicity study as a positive control[70–72]. Furthermore, **MM124** and **MM125** used in the highest concentrations (2 μM) induced similar levels of DNA damage compared to bleomycin used at 10 times higher concentration (20 μM). However, only **MM124** used in 1 μM concentration induced a statistically significant increase in DNA damage in both cancer cell lines (HT-29 and PC-3) but not normal cells (PBLs).

For the first time, we have evaluated the DNA interacting potential of pyrazolo[4,3-*e*][1,2,4]triazine which could potentially indicate the underlying basis of their genotoxic properties. Evaluating the type of occurring interaction using electrochemical techniques should be generally supplemented with other methods, as these techniques only allow for the formulation of a hypothesis based on the observed shift in peak potential. Here, the absence of shifts in the peak potentials suggests that intercalative type of interactions likely did not occur. Therefore, groove binding may be suggested as more prevalent.

Compound	Cell line							
	IC_{50} value							
	R	BxPC-3	PC-3	HeLa	DLD-1	HCT116	HT-29	WI-28	PBMCs
MM124	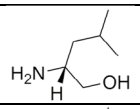	0.32	0.3	N/D	0.49	0.38	0.22	0.98	0.87
MM125	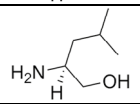	0.21	0.43	N/D	0.55	0.49	0.27	1.21	1.11
MM129	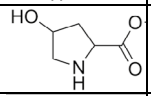	0.26	0.36	0.9	3.1#	0.6	3.1#	N/D	1.11
MM130	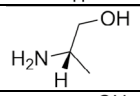	0.17	0.22	0.59	N/D	0.44	N/D	N/D	0.77
MM131	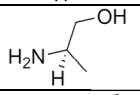	0.13	0.17	0.41	3.4#	0.39	3.9#	N/D	0.62
MM134	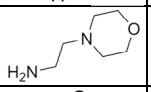	0.32	0.16	N/D	0.27*	0.38	0.2*	0.65	N/D
MM136	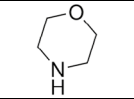	0.25	0.13	N/D	0.13*	0.25	0.12*	0.48	N/D
MM137	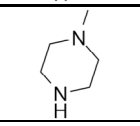	0.16	0.11	N/D	0.08*	0.14	0.08*	0.27	N/D
MM139	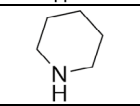	0.33	0.17	N/D	0.12*	0.35	0.09*	0.64	N/D

Table 8. Results of the MTT assay for MM-compounds documented in the literature. The cytotoxic properties of compounds were documented across various cancer cell lines, including BxPC-3 (pancreatic adenocarcinoma), PC-3 (prostate cancer), HeLa (cervical cancer), and DLD1/HCT116/HT29 (colorectal adenocarcinoma), as well as normal cells such as human lung fibroblasts (WI-38) and human peripheral blood mononuclear cells (PBMCs). The data were acquired following a 72-hour incubation of the cells with investigated sulfonamides (or 24 hours as denoted by the (#) symbol). N/D – not-determined; * - not-published data. Based on[76]

We have also performed in silico analysis of the compounds consisting of the ADMET properties prediction, molecular docking, and dynamics with DNA molecule to explore the binding mode of the compounds and the stability of the formed complexes. We have found that the compounds exhibit drug-likeness properties, do not show CYP inhibitory properties, and have favorable toxicity features, however, their use may be restricted by the low GI absorption. Docking and dynamics studies suggest the binding mode of the compounds as intercalative type. This could be attributed to the highly planar and hydrophobic nature of pyrazolo[4,3-*e*]tetrazolo[1,5-*b*][1,2,4]triazine core. However, distinct observations from the electrochemical and in silico studies need to be supplemented with other experimental approaches as described by other authors[73–75].

Our investigation complements the exploration of anti-cancer properties of pyrazolo[4,3-*e*]tetrazolo[1,5-*b*][1,2,4]triazine sulfonamides (**MM**-compounds series) designed and synthesized by Mojzych et al. that were extensively evaluated by several groups as recently described in our previous works[7,76]. The existing data on the cytotoxicity of the compounds was provided in Table 8. All the compounds in the series are characterized by the common pyrazolo[4,3-*e*]tetrazolo[1,5-*b*][1,2,4]triazine scaffold connected to specific amide heterocyclic moiety (R; see Table 8) by the phenylsulfonyl linker[24,69].

The data presented in Table 8 indicate that the incorporation of specific amide heterocyclic moieties does not appear to significantly influence the cytotoxic properties of the compounds in vitro. However, this structural modification profoundly impacts the physicochemical characteristics of the compounds, including ADMET profiles. These properties are challenging to fully evaluate through in vitro assays alone, necessitating further investigation through in vivo methods. The comparative evaluation of compound activity in cancerous versus normal cells is important for the assessment of the potential selectivity of chemical entities. Although the compounds exhibit only moderate selectivity in vitro, this differentiation is a critical starting point for therapeutic

development. Notably, preclinical studies on the advanced derivative **MM129** provided promising evidence that this class of heterocycles may possess anticancer efficacy in vivo, with an acceptable tolerability profile[22].

Recent studies have highlighted the potential for **MM**-derivatives to function synergistically with established anticancer agents. For example, combinatorial regimens involving **MM**- compounds with 5-FU[77] or the kynurenine pathway inhibitor—indoximod[78] have shown potential to enhance their therapeutic efficacy. This suggests that these compounds could be integrated into multidrug strategies to overcome resistance mechanisms and improve clinical outcomes. Future work should focus on further delineating the pharmacodynamics and pharmacokinetics of **MM**-derivatives, exploring their effects on tumor microenvironment, and validating their efficacy in diverse cancer models. Such studies are crucial to advancing these compounds toward clinical translation and understanding their full therapeutic potential.

Conclusions

In summary, the field of heterocyclic chemistry continues to evolve, offering numerous opportunities for novel drug discovery. Advances in synthesis methods and modern organic chemistry techniques have accelerated the development of new heterocyclic compounds with diverse biological activities[79–82]. Recent research has identified various pyrazolo-triazine derivatives with strong anticancer activity, particularly tricyclic pyrazolo[4,3-*e*][1,2,4] triazines fused with triazole or tetrazole rings[7,12,14,16,22–24,26,61,69]. Investigated here enantiomeric derivatives of pyrazolo[4,3-*e*]tetrazolo[1,5-*b*][1,2,4]triazine incorporating leucinol (**MM124** and **MM125**) exhibited comparable anticancer activity and similar cytotoxic properties to previously reported series of compounds. This indicates that incorporation of specific moieties with the phenylsulfonyl linker does not impact the biological activity of the pyrazolo[4,3-*e*]tetrazolo[1,5-*b*][1,2,4]triazine core. Nevertheless, both **MM**-compounds exhibited potent and selective cytotoxic activity against a panel of cancer cell lines derived from various tissue origins, with a median IC_{50} value of 0.35 μM. Mechanistic studies demonstrated that **MM124** and **MM125** induce apoptosis, promote oxidative stress, and cause DNA damage of prostate and colorectal cancer cells. Electrochemical analyses and molecular simulations further supported the ability of these compounds to interact with DNA. Additionally, in silico pharmacokinetic and toxicological evaluations indicated favorable drug-like properties, highlighting their potential for further development as anticancer agents.

Data availability

The data presented in this study are available in the main text of this article/supplementary materials of this article or on request from the corresponding author.

Received: 23 July 2024; Accepted: 16 May 2025
Published online: 28 May 2025

References

1. Cascioferro, S. et al. Synthesis and antitumor activities of 1,2,3-triazines and their benzo- and heterofused derivatives. *Eur. J. Med. Chem.* **142**, 74–86 (2017).
2. Rasková, H. & Zídek, Z. Surprises and omissions in toxicology. *Cent. Eur. J. Public Health* **12**(Suppl), S94-96 (2004).
3. Takagi, Y. & Otsuji, N. Studies on the mechanism of action of 6-azauracil. *Biochim. Biophys. Acta* **29**, 227–228 (1958).
4. Reddy, S. B. & Williamson, S. K. Tirapazamine: a novel agent targeting hypoxic tumor cells. *Expert Opin. Investig. Drugs* **18**, 77–87 (2009).
5. Brown, J. M. SR 4233 (tirapazamine): a new anticancer drug exploiting hypoxia in solid tumours. *Br. J. Cancer* **67**, 1163–1170 (1993).
6. Gucký, T., Frysová, I., Slouka, J., Hajdúch, M. & Dzubák, P. Cyclocondensation reaction of heterocyclic carbonyl compounds part XIII: synthesis and cytotoxic activity of some 3,7-diaryl-5-(3,4,5-trimethoxyphenyl)pyrazolo[4,3-e][1,2,4]triazines. *Eur. J. Med. Chem.* **44**, 891–900 (2009).
7. Bernat, Z., Szymanowska, A., Kciuk, M., Kotwica-Mojzych, K. & Mojzych, M. Review of the synthesis and anticancer properties of Pyrazolo[4,3-e][1,2,4]triazine derivatives. *Molecules* **25**, 3948 (2020).
8. Bouchain, G. & Delorme, D. Novel Hydroxamate and Anilide derivatives as potent histone deacetylase inhibitors: synthesis and antiproliferative evaluation. *Curr. Med. Chem.* **10**, 2359–2372 (2003).
9. Cheng, X.-C., Wang, Q., Fang, H. & Xu, W.-F. Role of sulfonamide group in matrix metalloproteinase inhibitors. *Curr. Med. Chem.* **15**, 368–373 (2008).
10. Lu, Y., Chen, J., Xiao, M., Li, W. & Miller, D. D. An overview of tubulin inhibitors that interact with the colchicine binding site. *Pharm. Res.* **29**, 2943–2971 (2012).
11. Mojzych, M., Dolashki, A. & Voelter, W. Synthesis of pyrazolo[4,3-e][1,2,4]triazine sulfonamides, novel sildenafil analogs with tyrosinase inhibitory activity. *Bioorg. Med. Chem.* **22**, 6616–6624 (2014).
12. Mojzych, M. et al. Synthesis of chiral pyrazolo[4,3-e][1,2,4]triazine sulfonamides with tyrosinase and urease inhibitory activity. *J. Enzyme Inhib. Med. Chem.* **32**, 99–105 (2017).
13. Scozzafava, A., Owa, T., Mastrolorenzo, A. & Supuran, C. T. Anticancer and antiviral Sulfonamides. *Curr. Med. Chem.* **10**, 925–953 (2003).
14. Mojzych, M. et al. Synthesis and kinase inhibitory activity of new sulfonamide derivatives of pyrazolo[4,3-e][1,2,4]triazines. *Eur. J. Med. Chem.* **78**, 217–224 (2014).
15. Cowan-Jacob, S. W. et al. Structural biology contributions to the discovery of drugs to treat chronic myelogenous leukaemia. *Acta Crystallogr. D Biol. Crystallogr.* **63**, 80–93 (2007).
16. Mojzych, M. et al. New pyrazolo[4,3-e][1,2,4]triazine sulfonamides as carbonic anhydrase inhibitors. *Bioorg. Med. Chem.* **23**, 3674–3680 (2015).
17. Byth, K. F. et al. Imidazo[1,2-b]pyridazines: a potent and selective class of cyclin-dependent kinase inhibitors. *Bioorg. Med. Chem. Lett.* **14**, 2249–2252 (2004).
18. Nie, Z. et al. Structure-based design, synthesis, and study of pyrazolo[1,5-a][1,3,5]triazine derivatives as potent inhibitors of protein kinase CK2. *Bioorg. Med. Chem. Lett.* **17**, 4191–4195 (2007).
19. Filhol, O. & Cochet, C. Protein kinase CK2 in health and disease: cellular functions of protein kinase CK2: a dynamic affair. *Cell. Mol. Life Sci. CMLS* **66**, 1830–1839 (2009).

20. Sciú, M. L. et al. Computer-aided molecular design of pyrazolotriazines targeting glycogen synthase kinase 3. *J. Enzyme Inhib. Med. Chem.* **34**, 87–96 (2019).
21. Hermanowicz, J. M. et al. Exploration of novel heterofused 1,2,4-triazine derivative in colorectal cancer. *J. Enzyme Inhib. Med. Chem.* **36**, 535–548 (2021).
22. Hermanowicz, J. M. et al. Preclinical Toxicity and Safety of MM-129-First-in-Class BTK/PD-L1 Inhibitor as a potential candidate against colon cancer. *Pharmaceutics* **13**, 1222 (2021).
23. Bukowski, K., Marciniak, B., Kciuk, M., Mojzych, M. & Kontek, R. Pyrazolo[4,3-e]tetrazolo[1,5-b][1,2,4]triazine Sulfonamides as novel potential anticancer agents: cytotoxic and genotoxic activities in vitro. *Molecules* **27**, 3761 (2022).
24. Kciuk, M. et al. Preparation of Novel Pyrazolo[4,3-e]tetrazolo[1,5-b][1,2,4]triazine Sulfonamides and Their Experimental and Computational Biological Studies. *Int. J. Mol. Sci.* **23**, 5892 (2022).
25. Mojzych, M. & Rykowski, A. Synthesis of functionalized 1H-Pyrazolo[4,3-e][1,2,4]triazines and their fused derivatives via Ipso-substitution of Methylsulfonyl group with O-, N-. *S- and C-Nucleophiles. Heterocycles* **63**, 1829–1838 (2004).
26. Gornowicz, A., Szymanowska, A., Mojzych, M., Bielawski, K. & Bielawska, A. The Effect of Novel 7-methyl-5-phenyl-pyrazolo[4,3-e]tetrazolo[4,5-b][1,2,4]triazine Sulfonamide derivatives on apoptosis and autophagy in DLD-1 and HT-29 colon cancer cells. *Int. J. Mol. Sci.* **21**, 5221 (2020).
27. Stockert, J. C., Horobin, R. W., Colombo, L. L. & Blázquez-Castro, A. Tetrazolium salts and formazan products in cell biology: Viability assessment, fluorescence imaging, and labeling perspectives. *Acta Histochem.* **120**, 159–167 (2018).
28. Grela, E., Kozłowska, J. & Grabowiecka, A. Current methodology of MTT assay in bacteria - A review. *Acta Histochem.* **120**, 303–311 (2018).
29. Da Violante, G. et al. Evaluation of the cytotoxicity effect of dimethyl sulfoxide (DMSO) on Caco2/TC7 colon tumor cell cultures. *Biol. Pharm. Bull.* **25**, 1600–1603 (2002).
30. Deshwal, S., Antonucci, S., Kaludercic, N. & Di Lisa, F. Measurement of mitochondrial ROS formation. *Methods Mol. Biol. Clifton NJ* **1782**, 403–418 (2018).
31. Xiao, B., Deng, X., Zhou, W. & Tan, E.-K. Flow cytometry-based assessment of Mitophagy using MitoTracker. *Front. Cell. Neurosci.* **10**, 76 (2016).
32. Hans, C., Saini, R., Sachdeva, M. U. S. & Sharma, P. 2',7'-Dichlorofluorescein (DCF) or 2',7'-dichlorodihydrofluorescein diacetate (DCFH2-DA) to measure reactive oxygen species in erythrocytes. *Biomed. Pharmacother. Biomedecine Pharmacother.* **138**, 111512 (2021).
33. Kim, H. & Xue, X. Detection of total reactive oxygen species in adherent cells by 2',7'-Dichlorodihydrofluorescein diacetate staining. *J. Vis. Exp. JoVE* **160**, e60682. https://doi.org/10.3791/60682 (2020).
34. Cordelli, E., Bignami, M. & Pacchierotti, F. Comet assay: a versatile but complex tool in genotoxicity testing. *Toxicol. Res.* **10**, 68–78 (2021).
35. Muruzabal, D., Collins, A. & Azqueta, A. The enzyme-modified comet assay Past, present and future. *Food Chem. Toxicol. Int. J. Publ. Br. Ind. Biol. Res. Assoc.* **147**, 111865 (2021).
36. Owiti, N. A., Nagel, Z. D. & Engelward, B. P. Fluorescence Sheds Light on DNA Damage, DNA Repair, and Mutations. *Trends Cancer* **7**, 240–248 (2021).
37. Møller, P. et al. Minimum information for reporting on the comet assay (MIRCA): recommendations for describing comet assay procedures and results. *Nat. Protoc.* **15**, 3817–3826 (2020).
38. Singh, N. P., McCoy, M. T., Tice, R. R. & Schneider, E. L. A simple technique for quantitation of low levels of DNA damage in individual cells. *Exp. Cell Res.* **175**, 184–191 (1988).
39. Pires, D. E. V., Blundell, T. L. & Ascher, D. B. pkCSM: predicting small-molecule pharmacokinetic and toxicity properties using graph-based signatures. *J. Med. Chem.* **58**, 4066–4072 (2015).
40. Daina, A., Michielin, O. & Zoete, V. SwissADME: a free web tool to evaluate pharmacokinetics, drug-likeness and medicinal chemistry friendliness of small molecules. *Sci. Rep.* **7**, 42717 (2017).
41. Canals, A., Purciolas, M., Aymamí, J. & Coll, M. The anticancer agent ellipticine unwinds DNA by intercalative binding in an orientation parallel to base pairs. *Acta Crystallogr. D Biol. Crystallogr.* **61**, 1009–1012 (2005).
42. Wu, X., Xu, L.-Y., Li, E.-M. & Dong, G. Application of molecular dynamics simulation in biomedicine. *Chem. Biol. Drug Des.* **99**, 789–800 (2022).
43. Singh, V., Mujwar, S., Singh, M., Singh, T. & Ahmad, S. F. Computational studies to understand the neuroprotective mechanism of action basil compounds. *Molecules* **28**, 7005 (2023).
44. Hollingsworth, S. A. & Dror, R. O. Molecular dynamics simulation for All. *Neuron* **99**, 1129–1143 (2018).
45. Chazotte, B. Labeling mitochondria with MitoTracker dyes. *Cold Spring Harb. Protoc.* **2011**, 990–992 (2011).
46 Kasibhatla, S. et al. Acridine Orange/Ethidium Bromide (AO/EB) Staining to Detect Apoptosis. *CSH Protoc.* **2006**, prot4493 (2006).
47. Lema, C., Varela-Ramirez, A. & Aguilera, R. J. Differential nuclear staining assay for high-throughput screening to identify cytotoxic compounds. *Curr. Cell. Biochem.* **1**, 1–14 (2011).
48. Gyori, B. M., Venkatachalam, G., Thiagarajan, P. S., Hsu, D. & Clement, M.-V. OpenComet: an automated tool for comet assay image analysis. *Redox Biol.* **2**, 457–465 (2014).
49. Zavazalova, J., Prochazkova, K. & Schwarzova-Peckova, K. Boron-doped diamond electrodes for Voltammetric determination of Benzophenone-3. *Anal. Lett.* **49**, 80–91 (2016).
50. Gosser, D. K. & Jr., VCH, New York, N. Y,. Cyclic voltammetry; simulation and analysis of reaction mechanisms:1993. *Synth. React. Inorg. Met. Org. Chem.* **24**, 1237–1238 (1994).
51. Schinkel, null.,. P-Glycoprotein, a gatekeeper in the blood-brain barrier. *Adv. Drug Deliv. Rev.* **36**, 179–194 (1999).
52. Zhao, M. et al. Cytochrome P450 enzymes and drug metabolism in humans. *Int. J. Mol. Sci.* **22**, 12808 (2021).
53. Siramshetty, V. B. et al. WITHDRAWN–a resource for withdrawn and discontinued drugs. *Nucleic Acids Res.* **44**, D1080-1086 (2016).
54. Zeiger, E. The test that changed the world: The Ames test and the regulation of chemicals. *Mutat. Res. Genet. Toxicol. Environ. Mutagen.* **841**, 43–48 (2019).
55. Lee, H.-M. et al. Computational determination of hERG-related cardiotoxicity of drug candidates. *BMC Bioinformatics* **20**, 250 (2019).
56. Descotes, J. Immunotoxicology: role in the safety assessment of drugs. *Drug Saf.* **28**, 127–136 (2005).
57. Nussbaumer, S., Bonnabry, P., Veuthey, J.-L. & Fleury-Souverain, S. Analysis of anticancer drugs: a review. *Talanta* **85**, 2265–2289 (2011).
58. Bukowski, K., Kciuk, M. & Kontek, R. Mechanisms of multidrug resistance in cancer chemotherapy. *Int. J. Mol. Sci.* **21**, 3233 (2020).
59. Mokhtari, R. B. et al. Combination therapy in combating cancer. *Oncotarget* **8**, 38022–38043 (2017).
60. Luqmani, Y. A. Mechanisms of drug resistance in cancer chemotherapy. *Med. Princ. Pract Int. J. Kuwait Univ. Health Sci. Cent.* **14**, 35–48 (2005).
61. Szymanowska, A. et al. The activity of pyrazolo[4,3-e][1,2,4]triazine and pyrazolo[4,3-e]tetrazolo[1,5-b][1,2,4]triazine sulphonamide derivatives in monolayer and spheroid breast cancer cell cultures. *J. Enzyme Inhib. Med. Chem.* **39**, 2343352 (2024).
62. Singh, A. K. et al. Concept of hybrid drugs and recent advancements in anticancer hybrids. *Pharmaceuticals* **15**, 1071 (2022).

63. Shi, F. et al. Synthesis, biological and pharmacokinetic characterization of a novel leucine Ureido derivative as a multi-target anticancer agent. *RSC Adv.* **15**, 4348–4355 (2025).
64. Yang, H. et al. Inhibition of the proliferation, migration, and invasion of human breast cancer cells by leucine aminopeptidase 3 inhibitors derived from natural marine products. *Anticancer. Drugs* **31**, 60–66 (2020).
65. Cao, J. et al. Leucine Ureido derivatives as aminopeptidase N inhibitors using click chemistry. *Part II. Bioorg. Med. Chem.* **27**, 978–990 (2019).
66. de Castro, P. P. et al. Cytotoxic activity of synthetic chiral amino acid derivatives. *J. Braz. Chem. Soc.* **31**, 193–200 (2020).
67. Lee, Y. et al. Structural basis of anticancer drug recognition and amino acid transport by LAT1. *Nat. Commun.* **16**, 1635 (2025).
68. Kciuk, M. et al. Synthesis, computational, and anticancer in vitro investigations of Aminobenzylnaphthols derived from 2-Naphtol, Benzaldehydes, and α-Aminoacids via the Betti reaction. *Mol. Basel Switz.* **28**, 7230 (2023).
69. Kciuk, M. et al. Genotoxicity of novel Pyrazolo[4,3-e]tetrazolo[1,5-b][1,2,4]triazine Sulfonamides in normal and cancer cells in vitro. *Int. J. Mol. Sci.* **24**, 4053 (2023).
70. Czaja, M. et al. Raman research on bleomycin-Induced DNA strand breaks and repair processes in living cells. *Int. J. Mol. Sci.* **23**, 3524 (2022).
71. Chen, J., Ghorai, M. K., Kenney, G. & Stubbe, J. Mechanistic studies on bleomycin-mediated DNA damage: multiple binding modes can result in double-stranded DNA cleavage. *Nucleic Acids Res.* **36**, 3781–3790 (2008).
72. Mohammed, S. M. et al. Mechanisms of bleomycin-induced lung fibrosis: a review of therapeutic targets and approaches. *Cell Biochem. Biophys.* **82**, 1845–1870. https://doi.org/10.1007/s12013-024-01384-9 (2024).
73. Mukherjee, A. & Sasikala, W. D. Drug-DNA intercalation: from discovery to the molecular mechanism. *Adv. Protein Chem. Struct. Biol.* **92**, 1–62 (2013).
74. Palchaudhuri, R. & Hergenrother, P. J. DNA as a target for anticancer compounds: methods to determine the mode of binding and the mechanism of action. *Curr. Opin. Biotechnol.* **18**, 497–503 (2007).
75. Venugopal, S., Sharma, V., Mehra, A., Singh, I. & Singh, G. DNA intercalators as anticancer agents. *Chem. Biol. Drug Des.* **100**, 580–598 (2022).
76. Kciuk, M. et al. Pyrazolo[4,3-e]tetrazolo[1,5-b][1,2,4]triazine Sulfonamides as an important scaffold for anticancer drug discovery-in vitro and in silico evaluation. *Int. J. Mol. Sci.* **24**, 10959 (2023).
77. Hermanowicz, J. M. et al. MM-129 as a novel inhibitor targeting PI3K/AKT/mTOR and PD-L1 in colorectal cancer. *Cancers* **13**, 3203 (2021).
78. Kwiatkowska, I. et al. Assessment of an anticancer effect of the simultaneous administration of MM-129 and indoximod in the colorectal cancer model. *Cancers* **16**, 122 (2023).
79. Kumar, D. & Jain, S. K. A comprehensive review of N-Heterocycles as cytotoxic agents. *Curr. Med. Chem.* **23**, 4338–4394 (2016).
80. Kumar, N. & Goel, N. Heterocyclic compounds: importance in anticancer drug discovery. *Anticancer Agents Med. Chem.* **22**, 3196–3207 (2022).
81. Broughton, H. B. & Watson, I. A. Selection of heterocycles for drug design. *J. Mol. Graph. Model.* **23**, 51–58 (2004).
82. Biswas, T., Mittal, R. K., Sharma, V. & Kanupriya, null & Mishra, I.,. Nitrogen-fused heterocycles: empowering anticancer drug discovery. *Med. Chem. Shariqah U. A. E.* **20**, 369–384. https://doi.org/10.2174/0115734064278334231211054053 (2024).

Acknowledgements

We would like to express our sincere gratitude to Professor Anna Zawisza from the Faculty of Chemistry, University of Lodz for her valuable time, insightful feedback, and constructive review of this work.

Author contributions

Conceptualization — M.K.; writing (original draft preparation) — M.K., G.M., S.M., B.M., K.K., and S.S.; writing (review and editing) — M.K., S.S., and M.M.; supervision — M.M. and R.K.

Declarations

Competing interests

The authors declare no competing interests.

Research involving human participants

The use of a human leucocyte buffy-coat was approved by the Bioethics Committee for Scientific Investigation, University of Lodz (agreement no. KBBN-UŁ/I/8/2019).

Additional information

Supplementary Information The online version contains supplementary material available at https://doi.org/10.1038/s41598-025-02835-w.

Correspondence and requests for materials should be addressed to M.K.